haematologica
Journal of the Ferrata Storti Foundation

IKZF1 gene deletions drive resistance to cytarabine in B-cell precursor acute lymphoblastic leukemia

by Britt M.T. Vervoort, Miriam Butler, Kari J.T. Grünewald, Dorette S. van Ingen Schenau, Trisha M. Tee, Luc Lucas, Alwin D.R. Huitema, Judith M. Boer, Beat M. Bornhauser, Jean-Pierre Bourquin, Peter M. Hoogerbrugge, Vincent H.J. Van der Velden, Roland P. Kuiper, Laurens T. van der Meer, and Frank N. van Leeuwen

Received: September 23, 2023.
Accepted: May 22, 2024.

Citation: Britt M.T. Vervoort, Miriam Butler, Kari J.T. Grünewald, Dorette S. van Ingen Schenau, Trisha M. Tee, Luc Lucas, Alwin D.R. Huitema, Judith M. Boer, Beat M. Bornhauser, Jean-Pierre Bourquin, Peter M. Hoogerbrugge, Vincent H.J. Van der Velden, Roland P. Kuiper, Laurens T. van der Meer, and Frank N. van Leeuwen. IKZF1 gene deletions drive resistance to cytarabine in B-cell precursor acute lymphoblastic leukemia. Haematologica. 2024 June 6. doi: 10.3324/haematol.2023.284357 [Epub ahead of print]

IKZF1 gene deletions drive resistance to cytarabine in B-cell precursor acute lymphoblastic leukemia

Britt M. T. Vervoort[1*], Miriam Butler[1*], Kari J.T. Grünewald[1], Dorette S. van Ingen Schenau[1], Trisha M. Tee[1], Luc Lucas[2], Alwin D. R. Huitema[1,2,3], Judith M. Boer[1], Beat C. Bornhauser[4], Jean-Pierre Bourquin[4], Peter M. Hoogerbrugge[1], Vincent H.J. van der Velden[5], Roland P. Kuiper[1,6], Laurens T. van der Meer[1,#], Frank N. van Leeuwen[1,#]

*B.M.T.V and M.B contributed equally to this study
[#]F.N.v.L and L.T.v.d.M contributed equally to this study

[1]Princess Máxima Center for Pediatric Oncology, Utrecht, 3584 CS, the Netherlands
[2]Netherlands Cancer Institute, Amsterdam, The Netherlands
[3]Department of Clinical Pharmacy, University Medical Center Utrecht, Utrecht University, Utrecht, The Netherlands
[4]Department of Pediatric Oncology, Children's Research Centre, University Children's Hospital Zurich, Zurich, CH-8008, Switzerland
[5]Department of Immunology, Erasmus MC, University Medical Center Rotterdam, Rotterdam, The Netherlands
[6]Department of Genetics, Utrecht University Medical Center, Utrecht University, Utrecht The Netherlands

Running title: *IKZF1* deletions induce AraC resistance

Correspondence: Frank N. van Leeuwen, Heidelberglaan 25, Research building, 3rd floor, Room 3-4K1, 3584 CS Utrecht, The Netherlands; e-mail: F.N.vanleeuwen@prinsesmaximacentrum.nl

Data availability: RNA sequencing data generated in this study are publicly available in GEO at GSE234637, as well as the patient expression data via reference number GSE87070. The corresponding patient *IKZF1* status can be found in Supplemental Table 1. For R-scripts or any other material requests, please contact F.N.vanleeuwen@prinsesmaximacentrum.nl

Word count: 3999

Authorship Contributions

Contribution: B.M.T.V. designed and performed experiments, analyzed and interpreted the data and wrote the manuscript. M.B. designed and performed experiments of Figure 1 together with B.M.T.V. L.T.v.d.M. and F.N.v.L. initiated the project and supervised the work. K.G. analyzed datasets presented in Figure 3g and 4a-c, g as well as Supplemental Figure 4 and 5. D.S.v.I.S. performed experiments presented in Figure 1f-g, Figure 2a-b, and Supplemental Figure 2 and 3. T.M.T. supported data interpretation and experimental design of Figure 1-5. L.L. performed and interpreted the experiment in Figure 3a, supervised by A.D.R.H. J.M.B. supported analyses of the data presented in Figure 3g, 4g and Supplemental Figure 4b and 5d-e. B.C.B. and J.P.B. provided patient material used in Figure 1f-g and Supplemental Figure 2. V.H.J.v.d.V., P.M.H. and R.P.K. performed analyses and supervised the work on Figure 2c-e.

Acknowledgements: We are thankful to Didier Trono for providing psPAX2 (Addgene plasmid # 12260) and pMGD2 (Addgene plasmid # 12259). The pL-CRISPR.EFS.GFP and pLKO5.sgRNA.EFS.tRFP were a gift from Benjamin Ebert (Addgene plasmids # 57818 and 57823). The Human CRISPR enriched pooled library was a gift from David Sabatini & Eric Lander (Addgene #51044). We acknowledge the Utrecht Sequencing Facility (USEQ) for providing sequencing service and data. USEQ is subsidized by the University Medical Center Utrecht and The Netherlands X-omics Initiative (NWO project 184.034.019). We acknowledge Ruud Delwel, Leonie Smeenk and Marije Havermans for lively discussions about Evi1 and providing us with the K562 t(3.8) cells. We are grateful to the flow cytometry facility of the Princess Máxima Center and to the PRIME team of the Radboudumc animal facility for providing technical support.

Conflict of interest: The authors declare no conflict of interest

Financial Support: This work was supported in part by research funding from Dutch Cancer Society (KWF) (grant #10072, #11249 and #14659) and from Kika (grant #333). The authors declare no competing financial interests.

ABSTRACT

IKZF1-deletions occur in 10-15% of patients with B-cell precursor acute lymphoblastic leukemia (BCP-ALL) and predict a poor outcome. However, the impact of *IKZF1*-loss on sensitivity to drugs used in contemporary treatment protocols has remained underexplored. Here we show in experimental models and in patients that loss of *IKZF1* promotes resistance to AraC, a key component of both upfront and relapsed treatment protocols. We attribute this resistance, in part, to diminished import and incorporation of cytarabine (AraC) due to reduced expression of the solute carrier hENT1. Moreover, we find elevated mRNA expression of Evi1, a known driver of therapy resistance in myeloid malignancies. Finally, a kinase directed CRISPR/Cas9-screen identified that inhibition of either mediator kinases CDK8/19 or casein kinase 2 can restore response to AraC. We conclude that this high-risk patient group could benefit from alternative antimetabolites, or targeted therapies that re-sensitize the cells to AraC.

INTRODUCTION

With contemporary treatment protocols, close to 95% of all pediatric B cell precursor acute lymphoblastic leukemia (BCP-ALL) patients are cured(1). However, still about 10% of the pediatric BCP-ALL patients are confronted with relapsed disease(1). Moreover, the intense multi-agent chemotherapy regimen comes with many acute and long-term side effects as well as treatment-related mortality(2). While reduced intensity treatment for patients with favorable genetic profiles has been successfully introduced(3), options remain limited for high-risk leukemia subtypes, as the dose intensity of conventional chemotherapy has been pushed to its limit. This underscores the need for alternative more effective treatment strategies for high-risk BCP-ALL, which take into account leukemia specific drug sensitivity profiles(2).

Deletions or mutations affecting the lymphoid transcription factor *IKZF1* occur in approximately 10-15% of pediatric BCP-ALL patients and are associated with poor outcome(4-6). In about 80% of the *IKZF1*-deleted relapses, the *IKZF1*-deleted clone was preserved from diagnosis, suggesting that loss of *IKZF1* function contributes to therapy resistance(7). Loss of *IKZF1* function promotes cell intrinsic resistance to synthetic glucocorticoids(6, 8), which can be reversed by the use of small molecule inhibitors(9). To what extent loss of *IKZF1* function affects sensitivity to other drugs used in contemporary treatment protocols, has not been explored.

Here, we modelled loss of *IKZF1* function in BCP-ALL cell lines and patient derived xenografts (PDX) and compared cellular responses to various chemotherapeutic agents used in the treatment of BCP-ALL. We demonstrate that loss of *IKZF1* function is associated with Cytarabine (AraC) resistance and we investigate the underlying mechanisms.

METHODS

Detailed experimental descriptions can be found in the supplemental methods.

Ethical statement

Patient derived xenografts were generated from patient samples collected from different countries within the International BFM Study Group (I-BFM-SG) and the Dutch Childhood Oncology Group. All patients were enrolled in trials on treatment of pediatric BCP-ALL conducted by individual member groups of the I-BFM-SG: the AIEOP-BFM study group (Austria, Germany, Italy and Switzerland), the FRALLE study group (France) and the United Kingdom (UK) National Cancer Research Institute (NCRI) Childhood Cancer and Leukemia

Group and DOCG Group. All treatment trials were approved by the respective national institutional review boards, and informed consent for the use of spare specimens for research was obtained from study individuals, parents, or legal guardians.

RQ-PCR-based MRD analyses

MRD levels of patients treated within the ALL-10 or ALL-11 treatment protocol were routinely determined by real-time quantitative PCR (RQ-PCR) analysis of rearranged immunoglobulin (IG) and/or T-cell receptor (TR) gene rearrangements, and the laboratory participated in the quality control rounds of the EuroMRD network (see www.EuroMRD.org). RQ-PCR data, performed in triplicate, were analyzed according to the EuroMRD guidelines, using the criteria to prevent false-negative MRD results(10). To calculate the log reduction between time point 1(TP1, day 33) and time point 2 (TP2, day 79), patients with MRD levels $\geq 10^{-2}$ at TP1 were selected (providing 2 log steps for quantitative analysis). To allow calculations of log reduction, positive non-quantifiable MRD data ($<10^{-4}$) were arbitrarily set at a value of $5x10^{-5}$ and negative MRD data were set at $1x10^{-6}$. All MRD values were 10log-transformed, and the resulting values of TP2 were divided by these from TP1.

In vivo mouse trial

This study followed international, national, and/or institutional guidelines for humane animal treatment and complied with relevant legislation. Ethical approval was obtained from the Animal Experimental Committee of the Radboud University (RU-DEC-2019-0036). *IKZF1* mutated and wildtype BCP-ALL xenografts were intravenously injected with 1×10^{6} viable cells in 2 mice per patient sample. One mouse of each pair was treated with AraC for two weeks (5 days on, 2 days off) and the delay in leukemia formation was calculated as described in the supplemental methods.

Crispr/Cas9 screen

For this Crispr/Cas9 screen, cells were exposed to 30nM and 50nM for a duration of 22 days, all in triplicates. Cells were sequenced and enriched and depleted genes were identified using the MAGeCK Test algorithm (Galaxy Version 0.5.8.1) (Supplemental Table 2).

Statistical analyses

p-Values were considered statistically significant when $p<0.05$ and illustrated as following *$p<0.05$, **$p<0.01$, ***$p<0.001$, ****$p<0.0001$.

RESULTS

Loss of IKZF1 protects against AraC induced apoptosis

To investigate the potential effects of *IKZF1* loss of function on cellular drug responses, we performed a drug screen in the BCP-ALL cell line Sem where we modelled *IKZF1* loss-of-function. As demonstrated earlier(9), a bi-allelic CRISPR/Cas9 induced frameshift mutation resulted in a complete loss of protein expression (Figure 1a), which unlike a heterozygous mutation led to a stable genotype. Furthermore, no difference in cell growth was observed between *IKZF1*$^{-/-}$ and control cells (Supplemental Figure 1a), indicating that drug responses are not a consequence of a lower proliferation rate. These *IKZF1* knockout cells were exposed to a panel of drugs used in the treatment of BCP-ALL and sensitivity was determined by measuring cell numbers using the CyQuant dye and compared to control cells transduced with non-targeting gRNAs (Figure 1b). In addition to the expected resistance to the glucocorticoids prednisolone and dexamethasone, *IKZF1*$^{-/-}$ cells displayed a reduced response to two other drugs in the treatment protocol, AraC and vincristine (Figure 1c, Supplemental Figure 1b). We repeated this assay using a more specific cell death measurement by testing for membrane integrity using flow cytometric detection of the binding of amine reactive dyes. This assay confirmed a diminished efficacy of the nucleoside analogue AraC in addition to glucocorticoid resistance in this model (Figure 1d), while no effect on the response to vincristine was seen (data not shown). In addition to amine exposure, DNA fragmentation and PARP cleavage assays confirmed increased resistance to AraC treatment for *IKZF1*$^{-/-}$ cells (Supplemental Figure 2a,b).

Endogenous IKZF1 gene deletions as well as pharmacological targeting of Ikaros protein in BCP-ALL xenografts correlates with resistance against AraC ex vivo and in vivo

To validate our results in models that more closely reflect primary BCP-ALL, we compared the response to AraC in a panel of patient-derived xenografts (PDX), cultured on feeder layers of immortalized bone marrow stroma cells(11). First, we tested to what extent endogenous gene deletions of *IKZF1* affect AraC treatment response (Figure 1e). A panel of 16 BCP-ALL PDXs, each derived from samples obtained at diagnosis, being either wildtype for *IKZF1* (n=6) or carrying clonal *IKZF1* deletions (n=10), were incubated with increasing concentrations of AraC. After 3 days, cell viability was measured by staining with amine reactive dyes and quantified by flow cytometry. Data were plotted as dose-response curves (Figure 1f) and the area under the curve (AUC) (Supplemental figure 2c) was calculated as measure for sensitivity. Similar to our findings in the model cell line, *IKZF1*-deleted PDXs showed a significantly increased resistance to AraC compared to PDXs wild type for *IKZF1*.

In addition, we studied the effect of pharmacological modulation of *IKZF1* protein levels in PDX samples wildtype for *IKZF1* to rule out differences in genetic background and look at an isolated effect of *IKZF1* loss. For this, we used thalidomides, a class of immunomodulatory agents (IMiDs) that act by targeting the lymphoid transcription factors *IKZF1* and *IKZF3* for proteasome-mediated degradation by the $Cul4A^{CRBN}$ E3 ligase complex(12). These agents are used in the treatment of multiple myeloma and myeloid neoplasms such as myelodysplastic syndrome (MDS). We selected iberdomide, a highly *IKZF1* specific thalidomide in this class(13), and tested therapy response to AraC in seven BCP-ALL PDX models wildtype for *IKZF1* (Figure 1g, Supplemental figure 2d). Indeed, a 24-hour exposure to >10nM iberdomide led to an effective degradation of *IKZF1* protein expression in these PDXs and induced resistance to AraC in 6 out of 7 tested PDXs (Figure 1g, Supplemental figure 2d). In the one xenograft (Patient #3862) that showed no significant effect of iberdomide treatment on AraC therapy response, iberdomide-mediated *IKZF1* degradation appeared to be less effective (Supplemental figure 2d).

To show that the ex-vivo response to therapeutic drugs accurately reflects the sensitivity of *in vivo* treatment, we performed a mouse trial (Figure 2a). This experimental setup allows for a greater number of leukemia models to be tested at the same time, allowing better representation of the disease subtype(14). We selected a panel of 10 PDXs (n=4 wildtype for *IKZF1* and n=6 $IKZF1^{+/-}$) and injected each into 2 mice. Upon overt signs of leukemia, as measured by the presence of at least 1% of human cells in the blood (Supplemental figure 3a), one mouse of each pair was treated with AraC and leukemia development was compared to its untreated counterpart. By comparing the treatment induced delay in leukemia development, we established that *IKZF1* deleted PDX samples are less affected by AraC treatment in vivo (Figure 2b). Of note, the PDX samples that were most resistant *ex vivo* were also least affected by AraC treatment *in vivo,* highlighting the predictive value of ex vivo drug response profiling of patient derived cells in co-culture systems (Figure 1f, 2b and Supplemental figure 3b). Together, we find in PDX samples tested both *ex* and *in vivo* increased resistance towards AraC in samples harboring an *IKZF1* deletion similar to our cell line model.

BCP-ALL patients with IKZF1 gene alterations show a reduced response to an AraC-containing consolidation block

In contrast to our previous study where the response to glucocorticoids could be evaluated during a week-long single agent treatment(8), current protocols dictate the use of AraC in a combination with other drugs. This complicates the assessment of the relative contribution of

AraC. During the first consolidation phase of the recent Dutch ALL-10 and ALL-11 treatment protocols for pediatric BCP-ALL, patients are for the first time exposed to AraC, where they receive a cumulative dose of 1200 mg/m2 AraC(15, 16). Of note, in contemporary relapsed ALL protocols, higher doses of AraC are used. The consolidation block also contains 6-mercaptopurine (6-MP) 60 mg/m2/day p.o. for 28 days and 2 doses of 1000 mg/m2 cyclophosphamide(15, 17). Patients also received 1 or 2 doses of PEG-asparaginase and/or received 2 doses of intrathecal triple therapy (MTX, AraC and prednisolone at age-adjusted dosages) during this period. As this treatment block is flanked by minimal residual disease (MRD) measurements we were able to assess the effects of treatment on leukemia burden (Figure 2c). Since loss of *IKZF1* reduces response synthetic glucocorticoids(8), patients with *IKZF1* deleted leukemias show elevated MRD levels at the end of induction. To obtain a quantifiable MRD range for our comparison, we selected all patients with high MRD after induction at time point 1 as described in the Methods section. Because of this selection, MRD levels between *IKZF1*-deleted and *IKZF1* wildtype BCP-ALL patients at the start of the AraC containing treatment block did not differ (Figure 2d). To assess the potential effect of *IKZF1* deletions during consolidation, we analyzed the reduction of leukemia burden in MRD from TP1 (day 33) to TP2 (day 79). We observed that the fold reduction of MRD levels after the AraC containing therapy block was significantly lower for *IKZF1*-deleted patients compared to *IKZF1* wildtype patients, indicating increased treatment resistance in these patients (Figure 2e). Although we cannot exclude that reduced sensitivity for 6MP or other drugs may have contributed to these effects, we did not observe such a diminished response to asparaginase or 6MP in our *in vitro* assays (Figure 1c). We therefore attribute the observed resistance to AraC in these *IKZF1* deleted BCP-ALL patients.

Decreased hENT1 expression contributes to AraC resistance induced by IKZF1 loss

Most nucleoside analogues require active import and anabolic processing before the biologically active compound becomes available. This requirement poses a weakness that can be exploited by leukemia cells for development of resistance (Supplemental Figure 4a). Resistance to nucleoside analogs can be a consequence of ineffective cellular uptake, for instance due to reduced expression of nucleoside transporters, or changes in metabolic handling of these drugs(18). On the other hand, failed execution of apoptosis has also been reported in for example P53 null cells(19). To identify which of these mechanisms contributes to the resistance phenotype of *IKZF1* deleted cells, we used mass spectrometry to measure the incorporation of the active compound AraCTP in *IKZF1*$^{-/-}$ cells versus control Sem cells (Figure 3a). This showed a marked reduction of AraCTP incorporation in *IKZF1*

deleted cells. Previous studies have identified several proteins contributing to AraC incorporation into the DNA in AML (hENT1, dCK, CDA, 5NT, TOPO I, TOPO II, DNA POL and MDR1)(18, 20). To test whether any of these proteins contributed to *IKZF1*-mediated AraC-resistance we analyzed the relative expression of the genes encoding these proteins in *IKZF1*$^{-/-}$ cells relative to control Sem cells (Figure 3b). Only hENT1, the solute carrier that transports AraC over the cell membrane (Supplemental Figure 4a), showed a decreased mRNA expression in *IKZF1*$^{-/-}$ cells, which also translated into a decreased protein expression (Figure 3c-e). Indeed, overexpression of hENT1 in *IKZF1*$^{-/-}$ cells could sensitize cells to AraC treatment again (Supplemental figure 4b). Also iberdomide-mediated *IKZF1* degradation correlated with decreased hENT1 mRNA expression in 4 tested PDXs (Figure 3f). A trend towards lower hENT1 expression was also visible when we compared RNA sequencing data from primary patient material obtained at diagnosis (Figure 3g). Particularly in the B-other group, the subset that contains the majority of *IKZF1* deleted leukemias, lower hENT1 expression was seen in *IKZF1*-deficient samples, although the number of patients was too small to reach the statistical threshold (Supplemental Figure 4c). Together our experiments indicate that loss of hENT1 expression contributes to *IKZF1*-driven AraC therapy resistance.

Loss of IKZF1 promotes expression of oncogene Evi1

To obtain deeper insights into pathways or specific genes driving resistance to AraC upon loss of *IKZF1*, we performed RNA sequencing on samples from wildtype and *IKZF1* knockout Sem cells treated with and without AraC. We compiled a list of differentially expressed genes in response to treatment or as result of *IKZF1* loss (Figure 4a) and determined which KEGG pathways are overrepresented in this selection (Figure 4b, Supplemental Figure 5a). Three of the highest scoring pathways, focal adhesion, PI3K-AKT and MAPK, have previously been implicated in *IKZF1* mediated resistance to kinase inhibitor and glucocorticoid treatment(9, 21). Indeed, modulation of these pathways using the AKT inhibitor MK2206, the ERK inhibitor uprosertib or their combination enhanced the response to AraC, similar to what we have shown for prednisolone induced apoptosis(9) (Figure 4c). This corroboration of previous findings further strengthens the validity of our loss of function model. Since *IKZF1* functions as a repressive transcription factor, we focused on upregulated genes and pathways. *MECOM*, a gene annotated as component of the MAPK pathway (Figure 4d), caught our attention as it is frequently overexpressed in Acute Myeloid Leukemia (AML) where it dictates a poor outcome. *MECOM* encodes the zinc finger transcription factor Evi1, a prominent oncogene mostly known for its role in the pathogenesis of AML and Chronic Myeloid Leukemia (CML)(22), yet undefined for BCP-ALL. Evi1 is

essential for the maintenance of a stemness phenotype in hematopoietic stem cells(23). Several studies implicate Evi1 in AraC resistance in AML, suggesting a similar role for Evi1 in inducing resistance in BCP-ALL(24, 25). We used RT-qPCR to confirm that loss of *IKZF1* promotes expression of Evi1 in Sem cells and we observed that expression was further induced in response to AraC treatment (Figure 4e). A similar response was found in 4 out of 5 tested PDXs samples, where both Iberdomide-induced *IKZF1* degradation and AraC treatment promoted Evi1 expression (Figure 4f). Only in patient sample #3862 where iberdomide failed to effectively induce *IKZF1* degradation and AraC resistance (Supplemental figure 2d), Evi1 expression also did not elevate. Although Evi1 expression increased by 15-fold when *IKZF1* deleted Sem cells are treated with AraC, this expression is still ~50 fold lower as compared to AML cells carrying t(3::8)(q26::q24)translocation, the genetic event that most commonly results in upregulation of Evi1 in AML patients (Supplemental figure 5b,c). Although we were unable to detect Evi1 protein expression in our *IKZF1* knockout cells, these cells did not tolerate modulation of Evi1 protein levels as after shRNA mediated knockdown using 4 different shRNAs, these cells were rapidly lost from the culture within 2 days, while control cells continued to proliferate. This suggests that albeit expressed at low levels, Evi1 is essential for these *IKZF1* knockout cells to survive. Similar to what has been observed for AML cells(26), forced expression of Evi1 from a retrovirus also resulted in an immediate cell cycle arrest in our BCP-ALL models, while control cells continued to proliferate (data not shown). Of note, although we did not observe significant differences of Evi1 expression in RNA sequencing data from primary patient material, leukemias harboring *IKZF1* deletions were more likely to show high Evi1 expression, as defined by a chi-square test, compared to those wildtype for *IKZF1* (χ^2=5.574, *p=0.018) (Figure 4g, Supplemental Figure 5d). Similar to AML, BCP-ALL samples expressing high Evi1 levels showed increased mRNA expression of stem cell markers (Supplemental Figure 5e). Although the correlation between *IKZF1* mutations and elevated Evi1 expression may be dependent on co-occurring events, our data indicate that *IKZF1* loss may result in increased expression of Evi1 that, at least in a subset of leukemias, may contribute to a poor therapy response.

Inhibition of mediator kinases CDK8/19 or Casein Kinase II sensitizes the response to AraC

In search of druggable targets that could reverse AraC therapy resistance in *IKZF1* deleted ALL, we performed a CRISPR/Cas9-based loss-of-function screen with a sgRNA library targeting all human kinases (507) in Sem *IKZF1*$^{-/-}$ cells (Figure 5a). We performed 2 independent screens using low doses of AraC (30 nM and 50 nM) for 3 weeks allowing

selection of enriched or depleted sgRNAs (Supplemental Figure 6a,b). Using the MaGeCK algorithm(27), sgRNA counts between treated and untreated cells were compared. Of note, both screening conditions show a substantial overlap in the top ranked depleted and enriched genes, emphasizing the accuracy and reproducibility of this approach (Figure 5b, Supplemental Figure 6c, Supplemental Table 2).

We focused on depleted sgRNAs (dropouts), as loss of function of their target genes can be expected to enhance response to AraC. As expected, we found Akt1 as an enhancer of AraC response within the top 20 of depleted genes for both screening conditions (supplemental table 2), which confirms our earlier findings (Figure 4c). Among the highest scoring depleted genes in both screens, we identified the homologous cyclin dependent kinases CDK8/19. These mediator kinases regulate transcriptional programming and the metabolic homeostasis of cells and CDK8/19 inhibitors have been shown to prevent the development of resistance to different classes of drugs(28). To validate these targets, we used the small molecule inhibitor CCT251921, specifically targeting CDK8 and 19, at concentrations that marginally affect cell viability as a single agent, but in combination with AraC strongly synergized in both Sem wildtype and *IKZF1*$^{-/-}$ cells by decreasing IC_{50} values of ~5,2-fold at the highest concentration of the inhibitor (Figure 5d,e and Supplemental Figure 6d). Therefore, this combination therapy appears to enhance therapy response to AraC, independent of *IKZF1*-status.

In addition, we identified the sgRNAs targeting *CK2A1* and *CK2A2* among the strongest depleted genes in both screens (Figure 5b, Supplemental Figure 6c). *CK2* is known as casein kinase II and plays a prominent role in promoting cell growth, suppression of apoptosis and drug resistance in solid and hematological malignancies(29). More importantly, growing evidence shows that CK2 directly regulates transcription factor *IKZF1*(30). In case of hemizygous *IKZF1*-deletions in leukemia, inhibition of CK2 can restore the function of the intact *IKZF1* allele(31). It is therefore an interesting although unexpected hit in our CRISPR/Cas9 screen since the Sem *IKZF1*$^{-/-}$ cell line model has no intact allele left to restore, suggesting additional mechanisms taking place. It was shown that CK2 also phosphorylates Evi1 to enhance its activity, providing a potential explanation for the observed phenotype(32). As a validation of our CRISPR/Cas9 screen, we established that the CK2 inhibitor Silmitasertib synergized with AraC in both Sem wildtype cells and *IKZF1*$^{-/-}$ cells, although the highest synergy was observed in *IKZF1* deficient cells (IC_{50} decrease of ~2,3 fold in wildtype vs ~3,5 fold in *IKZF1*$^{-/-}$ cells), (Figure 5f, Supplemental Figure 6e). These findings indicate that inhibition of CK2, a modulator of both Evi1 and *IKZF1* activity, may offset the effects of *IKZF1* loss on AraC therapy resistance.

DISCUSSION

In this study we used genetic and pharmacological targeting of *IKZF1* to show that loss of *IKZF1* function reduces the response to AraC, a component of both upfront and relapsed BCP-ALL protocols. This observation contrasts with an earlier observation suggesting that *IKZF1* loss induces sensitivity to this nucleoside analog(33). However, our findings are corroborated by *in vitro* and *in vivo* studies using PDX and a retrospective analysis of MRD in patients. The insensitivity of *IKZF1* deleted cells may, at least in part, be the result of the reduced Ara-CTP incorporation (Figure 3a), a causality that was established already decades ago(34). We attribute this diminished incorporation, to a reduced availability of intracellular AraC because of lower hENT1 expression. The expression of this transporter is rate-limiting for AraC influx(35), particularly at the AraC concentrations that are used in the upfront treatment of BCP-ALL(36) and has been linked to AraC sensitivity in AML(37) and BCP-ALL(38). To improve treatment response in this high-risk leukemia subtype, patients might benefit from the selection of alternative nucleoside analogs that rely on the activity of other transporters, such as fludarabine or clofarabine.

In addition to controlling cellular metabolism, *IKZF1* is regarded as key regulator of lymphoid differentiation(39) while loss of *IKZF1* has been associated with stemness(40). In this context, the enhanced expression of the prominent oncogene Evi1 upon loss of *IKZF1* function is intriguing. Evi1 is essential for preventing differentiation of hematopoietic stem cells(41) and is best known for its role as an oncogene in myeloid leukemia. Overexpression of Evi1 is an independent poor prognostic factor in AML and associated with therapy resistance, including a decreased sensitivity to AraC(42, 43), but the prognostic value of high Evi1 expression in BCP-ALL remains unclear(44). We find upregulation of Evi1 mRNA expression upon genetic or pharmacological targeting of *IKZF1* (Figure 4c-e) while BCP-ALL samples displaying high Evi1 expression are enriched for leukemias with an *IKZF1* deletion. Although in publicly available ChIP-Seq datasets *IKZF1* does not seem to directly bind the *MECOM* locus(45), there are clear suggestions of a genetic interaction. Despite the facts that *IKZF1* aberrations are less common in AML, recurrent mutations are observed in (pediatric) AML and associated with poor outcome(46, 47). Moreover, isolated *IKZF1* deletions and monosomy 7 in AML appear to be enriched in Evi1-rearranged leukemias(48). Future studies should reveal whether Evi1 is directly suppressed by *IKZF1* or that the induction of Evi1 expression upon *IKZF1* loss is an indirect effect of the stem cell phenotype that is promoted by *IKZF1* loss(40). Moreover, the functional consequences of elevated Evi1 expression in *IKZF1* deleted leukemias and whether high Evi1 mRNA expression can serve as a potential biomarker for poor outcome in BCP-ALL remains to be established. Our model cell lines do not tolerate modulation of Evi1 itself, suggesting that this protein plays an

important role in cell survival and/or proliferation. Although Evi1 itself is not targetable, we show that inhibition of the upstream kinase CK2, a prominent hit in the CRISPR/Cas9-based loss-of-function screen which normally phosphorylates and activates both Evi1 and *IKZF1(30, 32)*, can reverse *IKZF1*-loss induced resistance to AraC. Together, it is an attractive hypothesis that the resistance phenotype of *IKZF1* deleted BCP-ALL and high expression of Evi1 is, at least in part, due to a genetic or functional interaction between *IKZF1* and Evi1.

Therapy resistance remains a formidable challenge in the treatment of cancer patients. In this study we identified multiple targetable mechanisms that may overcome drug resistance caused by loss of tumor suppressor *IKZF1*. Consistent with our previous observations(9), we find that targeting the MAPK pathway not only reverses glucocorticoid resistance but also increases sensitivity to AraC in *IKZF1* deleted leukemia. Additionally, we find that targeting CK2, the upstream activator of both *IKZF1* and Evi1, may represent an Achille's heel for *IKZF1*-mediated multidrug resistance. Although this clinically approved small molecule inhibitor is not yet used in the treatment of BCP-ALL, a quick translation to the clinic clinical application in BCP-ALL seems feasible(49). Another promising combination therapy involves drugs targeting the mediator kinases CDK8/19. Importantly, the sensitizing effects of these inhibitors are not limited to *IKZF1*-deleted cells, but also enhance AraC response in wildtype cells. Of note, CDK8/19 inhibitors are also under clinical investigation for the treatment of AML, albeit currently as a single agent(50). Therefore this combination therapy is not limited to BCP-ALL but could also be applied in the treatment of other malignancies such as AML, where AraC is a cornerstone drug playing a crucial role in achieving remission(51). Future *in vivo* experiments will have to demonstrate which of the identified targeted therapies will be most effective in reversing therapy resistance in *IKZF1* deleted BCP-ALL.

In conclusion, our study shows that loss of *IKZF1* induces resistance to AraC in BCP-ALL. This high-risk patient group may therefore benefit from alternative treatment strategies that either replace AraC or combine AraC with small molecule inhibitors that can re-sensitize cells to treatment.

REFERENCES

1. Reedijk AM, Coebergh JWW, de Groot-Kruseman HA, et al. Progress against childhood and adolescent acute lymphoblastic leukaemia in the Netherlands, 1990-2015. Leukemia. 2021;35(4):1001-1011.

2. Dixon SB, Chen Y, Yasui Y, et al. Reduced morbidity and mortality in survivors of childhood acute lymphoblastic leukemia: a report from the childhood cancer survivor study. J Clin Oncol. 2020;38(29):3418-3429.

3. Pieters R, de Groot-Kruseman H, Van der Velden V, et al. Successful therapy reduction and intensification for childhood acute lymphoblastic leukemia based on minimal residual disease monitoring: study ALL10 from the Dutch Childhood Oncology Group. J Clin Oncol. 2016;34(22):2591-2601.

4. Mullighan CG, Su X, Zhang J, et al. Deletion of IKZF1 and prognosis in acute lymphoblastic leukemia. N Engl J Med. 2009;360(5):470-480.

5. Kuiper R, Waanders E, Van Der Velden V, et al. IKZF1 deletions predict relapse in uniformly treated pediatric precursor B-ALL. Leukemia. 2010;24(7):1258-1264.

6. Steeghs EM, Boer JM, Hoogkamer AQ, et al. Copy number alterations in B-cell development genes, drug resistance, and clinical outcome in pediatric B-cell precursor acute lymphoblastic leukemia. Sci Rep. 2019;9(1):4634.

7. Yu J, Waanders E, van Reijmersdal SV, et al. Upfront treatment influences the composition of genetic alterations in relapsed pediatric B-cell precursor acute lymphoblastic leukemia. Hemasphere. 2020;4(1):e318.

8. Marke R, Havinga J, Cloos J, et al. Tumor suppressor IKZF1 mediates glucocorticoid resistance in B-cell precursor acute lymphoblastic leukemia. Leukemia. 2016;30(7):1599-1603.

9. Butler M, Vervoort BM, van Ingen Schenau DS, et al. Reversal of IKZF1-induced glucocorticoid resistance by dual targeting of AKT and ERK signaling pathways. Front Oncol. 2022;12:905665.

10. Van der Velden V, Cazzaniga G, Schrauder A, et al. Analysis of minimal residual disease by Ig/TCR gene rearrangements: guidelines for interpretation of real-time quantitative PCR data. Leukemia. 2007;21(4):604-611.

11. Frismantas V, Dobay MP, Rinaldi A, et al. Ex vivo drug response profiling detects recurrent sensitivity patterns in drug-resistant acute lymphoblastic leukemia. Blood. 2017;129(11):e26-e37.

12. Zhu YX, Braggio E, Shi C-X, et al. Identification of cereblon-binding proteins and relationship with response and survival after IMiDs in multiple myeloma. Blood. 2014;124(4):536-545.

13. Bjorklund CC, Kang J, Amatangelo M, et al. Iberdomide (CC-220) is a potent cereblon E3 ligase modulator with antitumor and immunostimulatory activities in lenalidomide-and pomalidomide-resistant multiple myeloma cells with dysregulated CRBN. Leukemia. 2020;34(4):1197-1201.

14. Murphy B, Yin H, Maris JM, et al. Evaluation of Alternative In Vivo Drug Screening Methodology: A Single Mouse AnalysisSingle Tumor Prediction of Tumor Response. Cancer Res. 2016;76(19):5798-5809.

15. Pieters R, de Groot-Kruseman H, Van der Velden V, et al. Successful therapy reduction and intensification for childhood acute lymphoblastic leukemia based on minimal residual disease monitoring: study ALL10 from the Dutch Childhood Oncology Group. J Clin Oncol. 2016;34(22):2591-2601.

16. Pieters R, de Groot-Kruseman H, Verwer F, et al. Dutch ALL11 Study: Improved Outcome for Acute Lymphoblastic Leukemia By Prolonging Therapy for IKZF1 Deletion and Decreasing Therapy for ETV6:: RUNX1, Down Syndrome and Prednisone Poor Responders. Blood. 2022;140(Supplement 1):519-520.

17. Pieters R, de Groot-Kruseman H, Fiocco M, et al. Improved Outcome for ALL by Prolonging Therapy for IKZF1 Deletion and Decreasing Therapy for Other Risk Groups. J Clin Oncol. 2023;41(25):4130-4142.

18. Galmarini CM, Mackey JR, Dumontet C. Nucleoside analogues: mechanisms of drug resistance and reversal strategies. Leukemia. 2001;15(6):875-890.

19. Feng L, Achanta G, Pelicano H, Zhang W, Plunkett W, Huang P. Role of p53 in cellular response to anticancer nucleoside analog-induced DNA damage. Int J Mol Med. 2000;5(6):597-604.

20. Galmarini CM, Thomas X, Calvo F, et al. In vivo mechanisms of resistance to cytarabine in acute myeloid leukaemia. Br J Haematol. 2002;117(4):860-868.

21. Churchman ML, Evans K, Richmond J, et al. Synergism of FAK and tyrosine kinase inhibition in Ph+ B-ALL. JCI insight. 2016;1(4):e86082.

22. Wieser R. The oncogene and developmental regulator EVI1: expression, biochemical properties, and biological functions. Gene. 2007;396(2):346-357.

23. Kataoka K, Sato T, Yoshimi A, et al. Evi1 is essential for hematopoietic stem cell self-renewal, and its expression marks hematopoietic cells with long-term multilineage repopulating activity. J Exp Med. 2011;208(12):2403-2416.

24. Bindels EMJ, Havermans M, Lugthart S, et al. EVI1 is critical for the pathogenesis of a subset of MLL-AF9–rearranged AMLs. Blood. 2012;119(24):5838-5849.

25. Masamoto Y, Chiba A, Takezaki T, et al. EVI1-Positive AML Cells Show Distinct Features and High Dependency on ETS Transcription Factor ERG. Blood. 2021;138(Supplement 1):784.

26. Lugthart S, Figueroa ME, Bindels E, et al. Aberrant DNA hypermethylation signature in acute myeloid leukemia directed by EVI1. Blood. 2011;117(1):234-241.

27. Li W, Xu H, Xiao T, et al. MAGeCK enables robust identification of essential genes from genome-scale CRISPR/Cas9 knockout screens. Genome Biol. 2014;15(12):554.

28. Sharko AC, Lim C-U, McDermott MS, et al. The inhibition of CDK8/19 mediator kinases prevents the development of resistance to EGFR-targeting drugs. Cells. 2021;10(1):144.

29. Buontempo F, McCubrey JA, Orsini E, et al. Therapeutic targeting of CK2 in acute and chronic leukemias. Leukemia. 2018;32(1):1-10.

30. Song C, Li Z, Erbe AK, Savic A, Dovat S. Regulation of Ikaros function by casein kinase 2 and protein phosphatase 1. World J Biol Chem. 2011;2(6):126-131.

31. Song C, Gowda C, Pan X, et al. Targeting casein kinase II restores Ikaros tumor suppressor activity and demonstrates therapeutic efficacy in high-risk leukemia. Blood. 2015;126(15):1813-1822.

32. Bard-Chapeau EA, Gunaratne J, Kumar P, et al. EVI1 oncoprotein interacts with a large and complex network of proteins and integrates signals through protein phosphorylation. Proc Natl Acad Sci U S A. 2013;110(31):E2885-E2894.

33. Rogers JH, Gupta R, Reyes JM, et al. Modeling IKZF1 lesions in B-ALL reveals distinct chemosensitivity patterns and potential therapeutic vulnerabilities. Blood Adv. 2021;5(19):3876-3890.

34. Kufe D, Spriggs D, Egan EM, Munroe D. Relationships among Ara-CTP pools, formation of (Ara-C) DNA, and cytotoxicity of human leukemic cells. Blood. 1984;64(1):54-58.

35. Wiley J, Jones S, Sawyer W, Paterson A. Cytosine arabinoside influx and nucleoside transport sites in acute leukemia. J Clin Invest. 1982;69(2):479-489.

36. Peters G, Schornagel J, Milano G. Clinical pharmacokinetics of anti-metabolites. Cancer Surv. 1993;17:123-156.

37. Candelaria M, Corrales-Alfaro C, Gutiérrez-Hernández O, et al. Expression levels of human Equilibrative nucleoside transporter 1 and Deoxycytidine kinase enzyme as prognostic factors in patients with acute myeloid leukemia treated with Cytarabine. Chemotherapy. 2016;61(6):313-318.

38. Ronald W, den Boer M, Meijerink J. Differential mRNA expression of Ara-C metabolizing enzymes explain Ara-C sensitivity in MLL gene-rearrengements infant acute lymphoblastic leukemia. Blood. 2003;101(4):1270-1276.

39. Marke R, van Leeuwen FN, Scheijen B. The many faces of IKZF1 in B-cell precursor acute lymphoblastic leukemia. Haematologica. 2018;103(4):565-574.

40. Li Z, Li S-P, Li R-Y, et al. Leukaemic alterations of IKZF1 prime stemness and malignancy programs in human lymphocytes. Cell Death Dis. 2018;9(5):526.

41. Kataoka K, Sato T, Yoshimi A, et al. Evi1 is essential for hematopoietic stem cell self-renewal, and its expression marks hematopoietic cells with long-term multilineage repopulating activity. J Exp Med. 2011;208(12):2403-2416.

42. Masamoto Y, Chiba A, Takezaki T, et al. EVI1-Positive AML Cells Show Distinct Features and High Dependency on ETS Transcription Factor ERG. Blood. 2021;138(Supplement 1):784.

43. Hinai AA, Valk PJ. Aberrant EVI 1 expression in acute myeloid leukaemia. Br J Haematol. 2016;172(6):870-878.

44. Nabil R, Abdellateif MS, Gamal H, et al. Clinical Significance of EVI-1 Gene Expression and Aberrations in Patient with De-Novo Acute Myeloid and Acute Lymphoid Leukemia. Leuk Res. 2023,126:107019.

45. Ferreirós-Vidal I, Carroll T, Taylor B, et al. Genome-wide identification of Ikaros targets elucidates its contribution to mouse B-cell lineage specification and pre-B–cell differentiation. Blood. 2013;121(10):1769-1782.

46. de Rooij JD, Beuling E, van den Heuvel-Eibrink MM, et al. Recurrent deletions of IKZF1 in pediatric acute myeloid leukemia. Haematologica. 2015;100(9):1151-1159.

47. Zhang X, Huang A, Liu L, et al. The clinical impact of IKZF1 mutation in acute myeloid leukemia. Exp Hematol Oncol. 2023;12(1):33.

48. Lavallée V-P, Gendron P, Lemieux S, D'Angelo G, Hébert J, Sauvageau G. EVI1-rearranged acute myeloid leukemias are characterized by distinct molecular alterations. Blood. 2015;125(1):140-143.

49. Grygier P, Pustelny K, Nowak J, et al. Silmitasertib (CX-4945), a clinically used CK2-kinase inhibitor with additional effects on GSK3β and DYRK1A kinases: a structural perspective. J Med Chem. 2023;66(6):4009-4024.

50. Borthakur GM, Donnellan WB, Solomon SR, et al. SEL120-a first-in-class CDK8/19 inhibitor as a novel option for the treatment of acute myeloid leukemia and high-risk myelodysplastic syndrome-data from preclinical studies and introduction to a phase Ib clinical trial. Blood. 2019;134(Supplement_1):2651.

51. Cros E, Jordheim L, Dumontet C, Galmarini CM. Problems related to resistance to cytarabine in acute myeloid leukemia. Leuk lymphoma. 2004;45(6):1123-1132.

FIGURE LEGENDS

Figure 1: Deletion of *IKZF1* drives resistance to AraC *in Vitro*

(a) Immunoblot analysis of *IKZF1* protein expression in single cell clones upon CRISPR/Cas9-based targeting of *IKZF1*. Representative blot of three independent experiments. **(b)** Schematic overview representing the workflow used to determine drug responses. Sem wildtype (WT) and Sem *IKZF1*-deleted cells were seeded into 384 wells plates and treated with drugs used in contemporary treatment protocols for pediatric B-cell precursor acute lymphoblastic leukemia (BCP-ALL) patients. After 3 days of incubation, cell death was analyzed by fluorescence intensity using the live cell staining CyQuant. **(c)** Fold change in cell viability (AUC) relative to cells wild type for *IKZF1* upon drug exposure. Corresponding dose response curves can be found in Supplemental Figure 1. **(d)** AraC induced cell death as determined by quantification of cells positive for amine-reactive dyes using flow cytometry in Sem wt and Sem *IKZF1* deleted cells after a 3-day treatment with increasing concentrations of AraC. (Mean ± standart error of the mean (SEM), n=3, ***p*=0.0011, T-test two sided based on AUC values). **(e)** Schematic overview representing the workflow used to determine ex-vivo drug responses in patient derived xenograft (PDX) samples. BCP-ALL PDX, either wildtype or carrying a heterozygous clonal deletion of *IKZF1* (*IKZF1*$^{+/-}$), were seeded on hTERT immortalized mesenchymal stem cells, allowed to settle for 24hr and then treated with increasing concentrations of AraC. After 3 days of incubation cell death was determined by quantification of cells positive for amine-reactive dyes using flow cytometry. **(f)** Cell viability determined by amine staining in patient derived xenografts either wild type (black, n=6) or carrying a heterozygous deletion (blue, n=10) of *IKZF1* as dose response curves. Of note, the least responsive WT sample, Patient #7148 harbors a t(17::19), a chromosomal translocation known to induce multiagent drug resistance and these patients have an extremely poor prognosis **(g)** Representative PDX sample for pharmacological targeting of the Ikaros protein using Iberdomide. Immunoblot analysis of *IKZF1* protein expression showing degradation of *IKZF1* protein in response to Iberdomide treatment after 24 hours. in different PDX samples. AraC induced cell death was determined by quantification of cells positive for amine-reactive dyes using flow cytometry after a 3-day treatment with increasing concentrations of AraC in the presence or absence of indicated doses of Iberdomide. Other tested PDX Samples (n=6) can be found in Supplemental figure 2d.

Figure 2: *IKZF1* deleted leukemias show resistance to AraC *in Vivo*

(a) Timeline of *in vivo* mouse trial. Each BCP-ALL PDX was injected into 2 mice at day 0 and leukemia growth was measured weekly by Flow Cytometry. At 1% of human cells in the blood, mice were treated for 2x 5 days with a break of 2 days in between, one of the pair receiving AraC and the other vehicle. Leukemia growth was traced weekly by Flow Cytometry and mice were sacrificed at >50% of human cells in the blood. **(b)** In vivo delay of leukemia growth upon AraC treatment in PDX wildtype for *IKZF1* and *IKZF1*$^{+/-}$ samples. (Mean ± SEM, **p*=0.034, T-test, two sided). **(c)** Schematic overview representing the workflow used to determine minimal residual disease (MRD) response in BCP-ALL patients in relation to *IKZF1*. Cases were selected that showed MRD levels >10^{-2} at timepoint 1 (TP1, day 33) and the response at timepoint 2 (TP2, day 79) was followed. **(d)** MRD levels at TP1 of patients wildtype for *IKZF1* (n=35) or patients carrying a heterozygous deletion of *IKZF1* (n=25). P=0.7867, Mann Whitney, two-tailed. **(d)** Ratio of MRD between TP1 and TP2 log10 transformed (TP1>TP2) of patients wildtype for *IKZF1* or carrying a heterozygous deletion of *IKZF1* after receiving a therapy block including AraC and 6-mercapto purine (6MP). (**p= 0.0065, Mann Whitney, two-tailed)

Figure 3: Decreased expression of solute carrier ENT1 observed upon loss of *IKZF1*

(a) Mass spectrometry was used to measure the DNA incorporated AraC in Sem wildtype vs Sem *IKZF1*$^{-/-}$ cells after treatment with AraC. The measurement of incorporation is expressed as ng AraC per ug 2dC after 24 hr and 72 hr of treatment with AraC. After 24hr 0,654 ng was measured in wildtype cells vs 0,552 ng in *IKZF1*$^{-/-}$ cells, z comparable ratio as found after 72hr where 1,78 ng and 1,47 ng was measured in wildtype vs *IKZF1*$^{-/-}$ cells. (Mean ± SEM, n=3, *p= 0.044 and *p=0.034 unpaired t-test, two-tailed). **(b)** Gene expression levels from RNAseq dataset, shown as Z-score, of genes associated with AraC resistance in either BCP-ALL or acute myeloid leukemia show a decreased expression of hENT1 in Sem *IKZF1*$^{-/-}$ cells versus control cells. **(c)** Validation of mRNA expression of hENT1 by RT-qPCR in Sem *IKZF1*$^{-/-}$ cells versus control cells. (Mean ± SEM, n=3, *p= 0.034, unpaired t-test two-tailed). **(d)** Representative western blot showing protein expression of hENT1 in Sem *IKZF1*$^{-/-}$ cells versus control cells. **(e)** Quantification of hENT1 Protein expression (Mean ± SEM, n=3, **p= 0.0059, unpaired t-test two-tailed). **(f)** mRNA expression of hENT1 by RT-qPCR in 4 different BCP-ALL PDX samples, pretreated with iberdomide for 24hr to break down the Ikaros Protein (Mean ± SEM, n=2 technical duplicate). **(g)** hENT1 expression in patients harboring an *IKZF1* deletion (n=100) versus patients wildtype for *IKZF1* (n=252), extracted from the GEO patient database (Ref: GSE87070). We included the BCP-ALL subtypes that have ≥ 3 *IKZF1*^{del} patients in this database, combining the B-other group, high hyperdiploid and BCR-ABL1 like.

Figure 4: Gene expression changes in the MAPK pathway reveal upregulated expression of Evi1 (*MECOM*) in *IKZF1*$^{-/-}$ cells

(a) Compiled heatmap created by unsupervised clustering of differential expressed genes to AraC treatment or as result of *IKZF1* loss from bulk RNA-seq data on Sem *IKZF1*$^{-/-}$ and control cells. Cells were treated with 1uM AraC for 16 hours and samples were harvested in triplicates. **(b)** KEGG pathway overrepresentation analysis was performed on the compiled list of differential expressed genes from a, showing here the 10 highest scoring pathways. **(c)** Cell viability determined in Sem *IKZF1*$^{+/-}$ and control cells by amine staining as dose response curves for AraC treatment in combination with AKT inhibitor MK2206 And ERK inhibitor Uprosertib. (Mean ± SEM, n=3, ***p*=0.0011, ANOVA followed by Tukey's multiple comparisons test.). **(d)** Heatmap created by unsupervised clustering of the MAPK pathway, only showing genes differentially expressed between control and *IKZF1*$^{-/-}$ cells upon AraC treatment. Heatmap is created using the FPKM values transformed into Z-scores. **(e)** Validation of Evi1 (*MECOM*) mRNA expression by RT-qPCR in Sem *IKZF1*$^{-/-}$ cells versus control cells upon treatment with 1uM AraC for 16 hours. (Mean ± SEM, n=3, ANOVA followed by Tukey's multiple comparisons test). **(f)** mRNA expression of *MECOM* by RT-qPCR in 5 different BCP-ALL PDX samples, pretreated with Iberdomide for 24hr. (Mean ± SEM, n=2 technical duplicate). **(g)** *MECOM* expression in patients harboring an *IKZF1* deletion (n=100) versus patients wildtype for *IKZF1* (n=352), extracted from the GEO database GSE87070. Here we included those BCP-ALL subtypes that counted ≥ 3 *IKZF1*^{del} patients in this database, combining here the B-other, BCR-ABL1 like and high hyperdiploid subgroups. A chi-square test was performed to calculate the correlation between IKZF1 mutations and elevated Evi1 expression (χ^2=5.574, *p=0.018).

Figure 5: CRISPR/Cas9 kinome screen revealing targetable genes to sensitize AraC treatment

(a) Schematic representation of our CRISPR screening strategy. Sem *IKZF1*$^{-/-}$ cells were transduced with a kinome sgRNA library and cultured for 2 weeks in the presence of 1 ug/mL Doxycyclin to induce Cas9 expression. Then, Cells were Split into 3 pools and treated for 22 days with either 0nM, 30nM or 50nM AraC. DNA was isolated and subjected to Illumina Next generation sequencing. **(b)** Vulcano-plot of sgRNA targets that significantly modulate AraC response, based on p-value and log fold change as analyzed using the MaGeCK Test algorithm. The top depleted genes are overlapping between the 30nM and 50nM AraC (supplemental figure 6C) screen as marked in red. **(c)** Counts of individual sgRNAs targeting CDK8, CDK19, CK2A1 and CK2A2 respectively between the untreated

cells and cells treated with 30nM AraC after screening for 22 days. **(d)** Combination therapy induced cell death as determined by quantification of cells positive for amine-reactive dyes using flow cytometry in Sem control and Sem *IKZF1*$^{-/-}$ cells after a 5-day treatment with increasing concentrations of AraC and CDK8/19 inhibitor CCT251921. Each data point represents a mean (+/- SEM) of 3 independent experiments. Two-way ANOVA is performed on the AUC values of the inhibitor in combination with AraC versus AraC as a single treatment, for both genotypes (***p<0.001, ****p<0.0001). Absolute IC_{50} values in wildtype cells is 80.8nM for AraC only versus 14.9nM in combination with 2uM CCT251921 respectively to 155.8nM for only AraC and 30.9nM for the combination in *IKZF1*$^{-/-}$ cells. **(e)** Synergy scores generated by Synergy finder software, using the values from figure 5D. **(f)** Combination therapy induced cell death as determined by quantification of cells positive for amine-reactive dyes using flow cytometry in Sem control and Sem *IKZF1*$^{-/-}$ cells after a 5-day treatment with increasing concentrations of AraC and CK2 inhibitor Silmitasertib. Each data point represents a mean (+/- SEM) of 3 independent experiments. Two-way ANOVA is performed on the AUC values of the inhibitor in combination with AraC versus AraC as a single treatment, for both genotypes (*p<0.05, **p<0.01, ***p<0.001, ****p<0.0001). Absolute IC_{50} values in wildtype cells is 35.9nM for AraC only versus 15.7nM in combination with 2uM CCT251921 respectively to 69.2nM for only AraC and 19.6nM for the combination in *IKZF1*$^{-/-}$ cells. **(g)** Synergy scores generated by Synergy finder software, using the values from figure 5D.

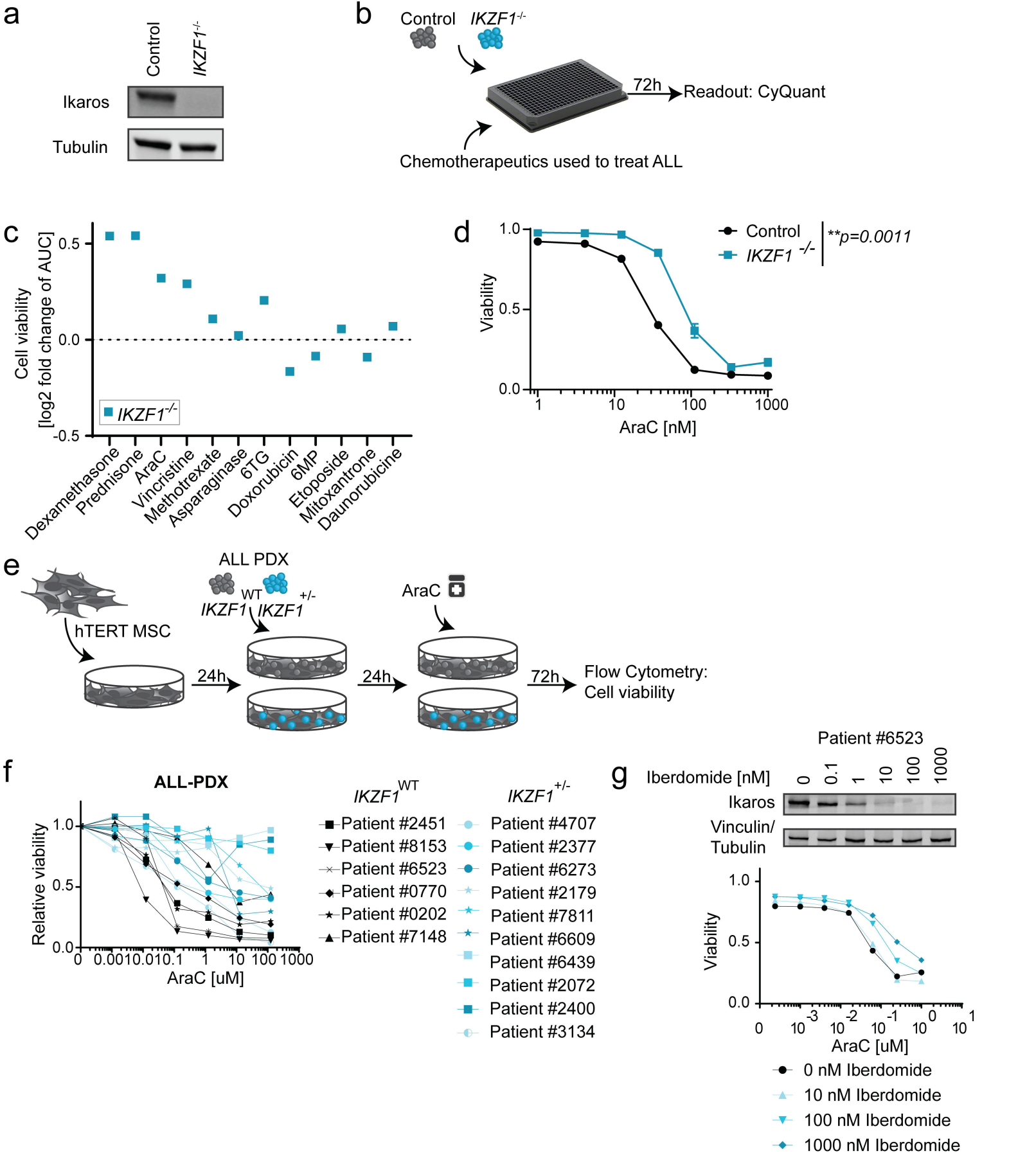
a
Control
IKZF1-/-
Ikaros
Tubulin
b
Control
IKZF1-/-
72h
Readout: CyQuant
Chemotherapeutics used to treat ALL
c
Cell viability
[log2 fold change of AUC]
0.5
0.0
-0.5
IKZF1-/-
Dexamethasone
Prednisone
AraC
Vincristine
Methotrexate
Asparaginase
6TG
Doxorubicin
6MP
Etoposide
Mitoxantrone
Daunorubicine
d
Viability
1.0
0.5
0.0
1
10
100
1000
AraC [nM]
Control
IKZF1 -/-
**p=0.0011
e
hTERT MSC
ALL PDX
IKZF1 WT
IKZF1 +/-
AraC
24h
24h
72h
Flow Cytometry:
Cell viability
f
ALL-PDX
Relative viability
1.0
0.5
0.0
0
0.001
0.01
0.1
1
10
100
1000
AraC [uM]
IKZF1WT
Patient #2451
Patient #8153
Patient #6523
Patient #0770
Patient #0202
Patient #7148
IKZF1+/-
Patient #4707
Patient #2377
Patient #6273
Patient #2179
Patient #7811
Patient #6609
Patient #6439
Patient #2072
Patient #2400
Patient #3134
g
Patient #6523
Iberdomide [nM]
0
0.1
1
10
100
1000
Ikaros
Vinculin/
Tubulin
Viability
1.0
0.5
0.0
0
10-3
10-2
10-1
100
101
AraC [uM]
0 nM Iberdomide
10 nM Iberdomide
100 nM Iberdomide
1000 nM Iberdomide

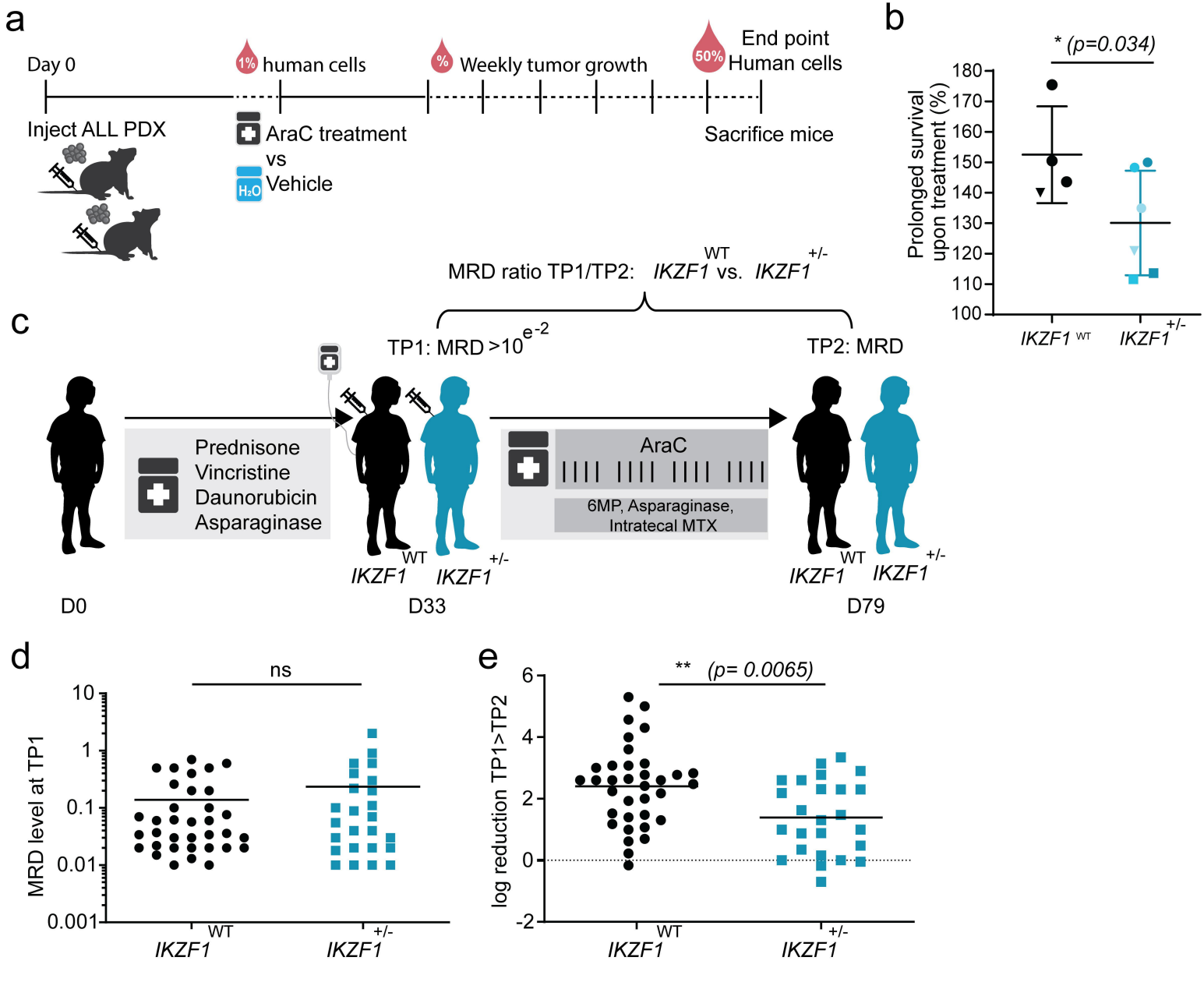
a
Day 0
1% human cells
% Weekly tumor growth
50% End point Human cells
Inject ALL PDX
AraC treatment
vs
Vehicle
Sacrifice mice
b
* (p=0.034)
Prolonged survival upon treatment (%)
180
170
160
150
140
130
120
110
100
IKZF1 WT
IKZF1 +/-
c
MRD ratio TP1/TP2: IKZF1 WT vs. IKZF1 +/-
TP1: MRD >10 e-2
TP2: MRD
Prednisone
Vincristine
Daunorubicin
Asparaginase
AraC
6MP, Asparaginase,
Intratecal MTX
IKZF1 WT
IKZF1 +/-
D0
D33
D79
d
ns
MRD level at TP1
10
1
0.1
0.01
0.001
IKZF1 WT
IKZF1 +/-
e
** (p= 0.0065)
log reduction TP1>TP2
6
4
2
0
-2
IKZF1 WT
IKZF1 +/-

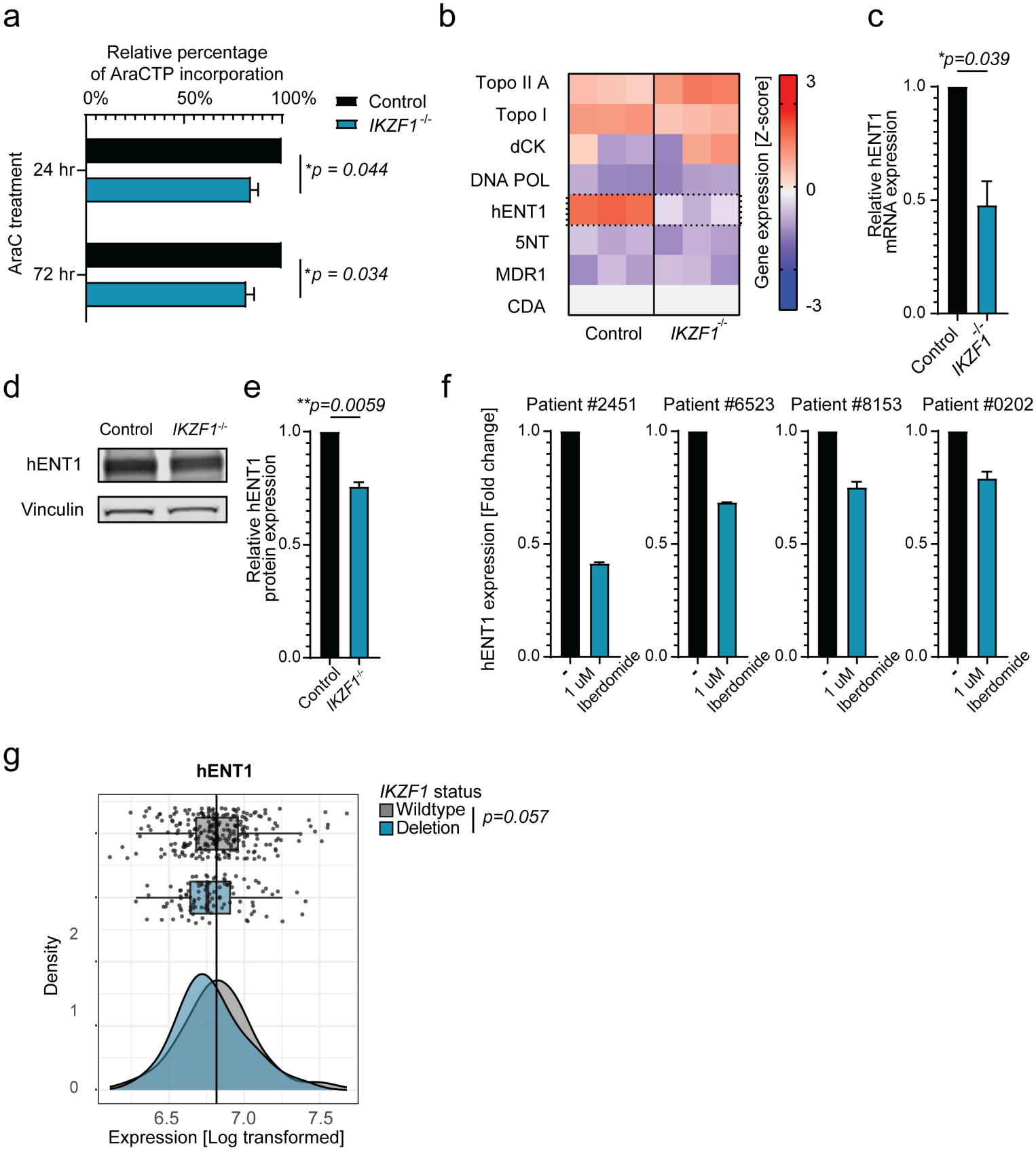
a
Relative percentage of AraCTP incorporation
0%
50%
100%
Control
IKZF1-/-
AraC treatment
24 hr
72 hr
*p = 0.044
*p = 0.034
b
Topo II A
Topo I
dCK
DNA POL
hENT1
5NT
MDR1
CDA
Control
IKZF1-/-
Gene expression [Z-score]
3
0
-3
c
*p=0.039
Relative hENT1 mRNA expression
1.0
0.5
0.0
Control
IKZF1-/-
d
Control
IKZF1-/-
hENT1
Vinculin
e
**p=0.0059
Relative hENT1 protein expression
1.0
0.5
0.0
Control
IKZF1-/-
f
Patient #2451
Patient #6523
Patient #8153
Patient #0202
hENT1 expression [Fold change]
1.0
0.5
0.0
-
1 uM Iberdomide
g
hENT1
IKZF1 status
Wildtype
Deletion
p=0.057
Density
2
1
0
6.5
7.0
7.5
Expression [Log transformed]

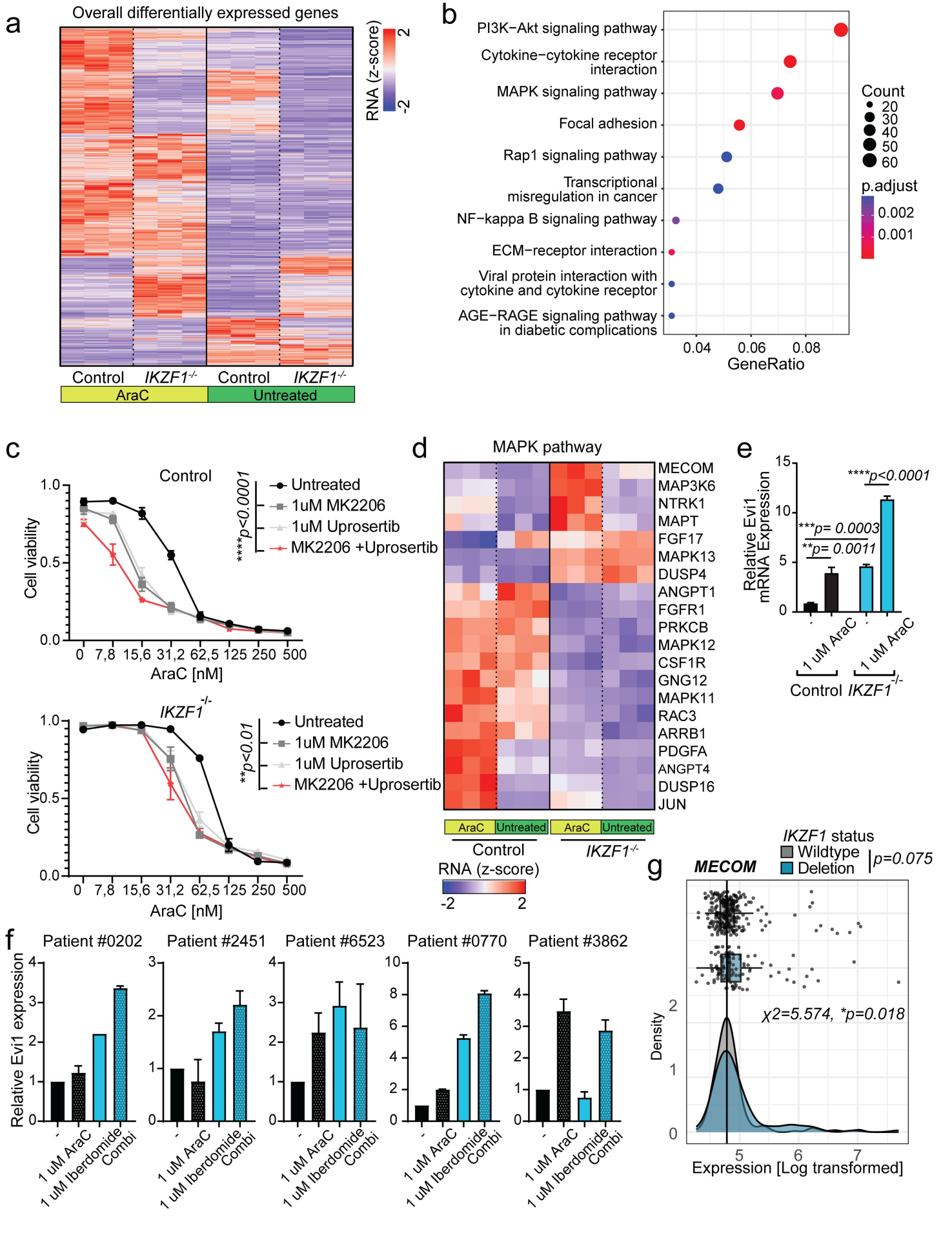
a
Overall differentially expressed genes
RNA (z-score)
2
-2
Control
IKZF1-/-
Control
IKZF1-/-
AraC
Untreated
b
PI3K−Akt signaling pathway
Cytokine−cytokine receptor interaction
MAPK signaling pathway
Focal adhesion
Rap1 signaling pathway
Transcriptional misregulation in cancer
NF−kappa B signaling pathway
ECM−receptor interaction
Viral protein interaction with cytokine and cytokine receptor
AGE−RAGE signaling pathway in diabetic complications
0.04
0.06
0.08
GeneRatio
Count
20
30
40
50
60
p.adjust
0.002
0.001
c
Control
Cell viability
1.0
0.5
0.0
0
7,8
15,6
31,2
62,5
125
250
500
AraC [nM]
****p<0.0001
Untreated
1uM MK2206
1uM Uprosertib
MK2206 +Uprosertib
IKZF1-/-
**p<0.01
Untreated
1uM MK2206
1uM Uprosertib
MK2206 +Uprosertib
d
MAPK pathway
MECOM
MAP3K6
NTRK1
MAPT
FGF17
MAPK13
DUSP4
ANGPT1
FGFR1
PRKCB
MAPK12
CSF1R
GNG12
MAPK11
RAC3
ARRB1
PDGFA
ANGPT4
DUSP16
JUN
AraC
Untreated
AraC
Untreated
Control
IKZF1-/-
RNA (z-score)
-2
2
e
Relative Evi1 mRNA Expression
15
10
5
0
****p<0.0001
***p= 0.0003
**p= 0.0011
-
1 uM AraC
-
1 uM AraC
Control
IKZF1-/-
f
Patient #0202
Patient #2451
Patient #6523
Patient #0770
Patient #3862
Relative Evi1 expression
-
1 uM AraC
1 uM Iberdomide
Combi
g
MECOM
IKZF1 status
Wildtype
Deletion
p=0.075
χ2=5.574, *p=0.018
Density
Expression [Log transformed]

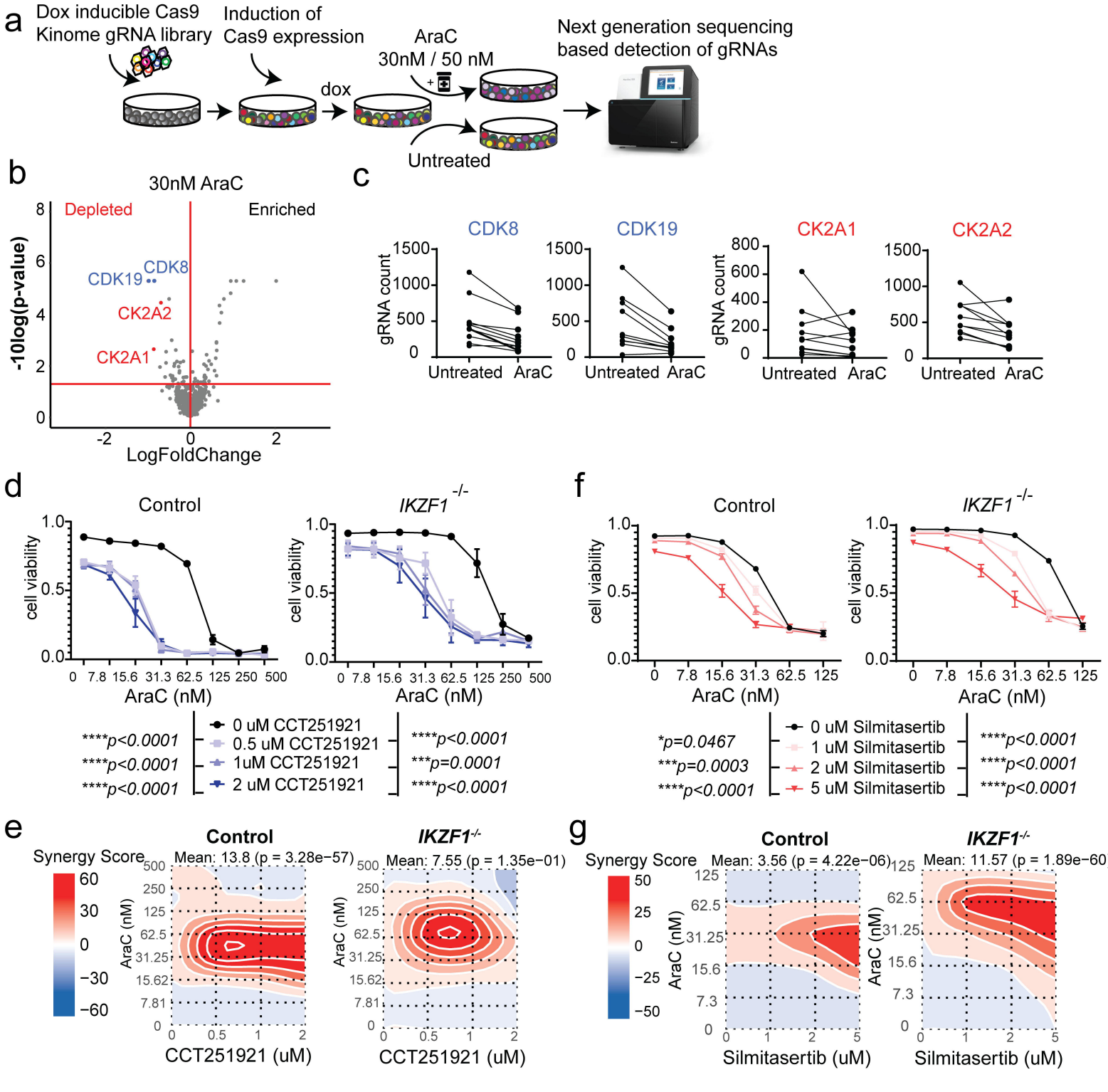
a
Dox inducible Cas9
Kinome gRNA library
Induction of
Cas9 expression
dox
AraC
30nM / 50 nM
Untreated
Next generation sequencing
based detection of gRNAs
b
30nM AraC
Depleted
Enriched
-10log(p-value)
LogFoldChange
CDK8
CDK19
CK2A2
CK2A1
c
CDK8
CDK19
CK2A1
CK2A2
gRNA count
Untreated
AraC
d
Control
IKZF1 -/-
cell viability
AraC (nM)
0 uM CCT251921
0.5 uM CCT251921
1uM CCT251921
2 uM CCT251921
****p<0.0001
****p<0.0001
****p<0.0001
****p<0.0001
***p=0.0001
****p<0.0001
f
Control
IKZF1 -/-
cell viability
AraC (nM)
0 uM Silmitasertib
1 uM Silmitasertib
2 uM Silmitasertib
5 uM Silmitasertib
*p=0.0467
***p=0.0003
****p<0.0001
****p<0.0001
****p<0.0001
****p<0.0001
e
Control
IKZF1-/-
Synergy Score
Mean: 13.8 (p = 3.28e−57)
Mean: 7.55 (p = 1.35e−01)
AraC (nM)
CCT251921 (uM)
g
Control
IKZF1-/-
Synergy Score
Mean: 3.56 (p = 4.22e−06)
Mean: 11.57 (p = 1.89e−60)
AraC (nM)
Silmitasertib (uM)

Supplemental File

SUPPLEMENTAL METHODS

Cell viability assays

Cell viability was determined using a MTS assay and flow cytometry using amine staining to discriminate between live and dead cells. For the MTS assay 100,000 cells were seeded in a well of a 96 well plate, flow cytometry cells were seeded in a 96-well plate, 24-well plate or in a 6-well plate at 500,000 cells per mL. After the indicated incubation times, relative cell viability was assessed using the CellTiter 2 96® AQueous One Solution Cell Proliferation (MTS) Assay (Promega, Madison, WI). Absorbance was acquired using a plate reader (Infinite F50; TECAN, Männedorf, Switzerland). Alternatively, cells were stained with LIVE/DEAD™ Fixable Dead Cell Stain Sampler Kit (Thermo-Fischer, L34960) according to the manufacturer's instructions or by incubating the cells with 7,5 µg/ml Hoechst 33342 (Sigma Aldrich (Zwijndrecht, the Netherlands) for 45 minutes at 37 °C in culture medium. Stained cells were analyzed by Fluorescence Activated Cell Sorting (FACS) using an LSRII flow cytometer (BD Biosciences, Breda, The Netherlands) or CytoFLEX LX (Beckman Coulter). For co-culture experiments, MSCs were gated out via FSC/SSC gating. The data were collected and analyzed by FlowJo V10 software (FlowJo, Ashland, Oregon).

Cell culture

Sem cells (ACC 546) were obtained from the Leibniz Institute DSMZ (German Collection of Microorganisms and Cell Cultures, Braunschweig, Germany) and K562 wildtype and t(3.8) were a gift from Ruud Delwel. Both cell lines are maintained in RPMI (Invitrogen, Thermo Fisher Scientific, Breda, the Netherlands), supplemented with 10% fetal bovine serum (FBS, Greiner Bio-One, Essen, Germany) and 1% penicillin/streptomycin solution (P/S) (Invitrogen) at a cell density between 0.2 and $3x10^6$ cells per milliliter. Cell line identity was confirmed by DNA fingerprinting.

Hek293FT cells were purchased from Invitrogen and maintained in DMEM, supplemented with 10% FBS, 1% Non-essential amino acids (Gibco, Thermo Fischer) and 1% P/S. Cell cultures were tested regularly for the presence of mycoplasma.

Plasmids

The following plasmids were obtained via Addgene: pS-Pax2 (#12260), pMGD2 (#12259), pL-CRISPR.EFS.GFP (#57818), pLKO5.sgRNA.EFS.tRFP (#57823). *IKZF1* KD plasmids were purchased from sigma (pLKO1-Puro). For targeted knockout, gRNA sequences (Supplemental Table 3) were cloned into pL-CRISPR.EFS.GFP and pLKO5.sgRNA.EFS.tRFP using the BsmBI sites and the resulting vector was verified using Sanger sequencing. The hENT1 overexpression vector was obtained from Twist Bioscience (San Francisco, California). The

hENT1 protein sequence (NP_001071643.1) was used as a template to generate and synthesize a DNA sequence that was cloned into the pTwist Lenti SFFV. Sequence was verified using Sanger sequencing. The empty plasmid was used as control.

Reagents

Cytarabine (AraC), Prednisone, Dexamethasone, Vincristine, Methotrexate, Asparaginase, 6TG, Doxorubicin, 6MP, Etoposide, Mitoxantrone, Daunorubicin were ordered from Selleckchem (Munich, Germany) and dissolved as instructed by the manufacturer.

Lentivirus production and transduction

HEK293FT packaging cells (Invitrogen) were co-transfected with a viral backbone encoding the sgRNAs or Cas9 and the helper plasmids for virus production (psPAX2 and pMD2.G), using Polyethylenimine (PEI). Virus containing supernatant was collected 2 days after transfection. Virus was concentrated by centrifugation at 25,000G for 1 hour at 4°C and resuspended in the cell culture medium required by the target cells. Target cells ($0.5\text{-}1x10^6$) were transduced with 1 mL virus (1-10 times concentrated) using spinoculation for 45 min at 700g (30°C) in the presence of 5 ug/mL polybrene (Santa Cruz Biotechnology, Dallas, TX). Selection was started 72-96 hours after transduction (2ug/mL puromycin) or GFP/RFP positive cells were sorted by Flow cytometry using the H800S Cell Sorter (Sony Biotechnology).

Real-time quantitative polymerase chain reaction

Total RNA was extracted using the RNeasy mini-kit (Qiagen). Subsequently, cDNA was synthesized of 500 ng RNA template using the iScriptTM cDNA synthesis kit (Bio-Rad, Hercules, CA). mRNA expression levels were determined by use of Power SYBR®Green PCR master mix using gene-specific primers (Supplemental table 4) and the CFX96 TouchTM Real-Time PCR detection system (Bio-Rad, Hercules, CA, USA). TBP mRNA expression was used as a reference to obtain the relative fold expression of target genes using the comparative cycle threshold 2(-ΔΔCt) method.

Immunoblotting

Cells were lysed in Laemmli protein buffer and treated with benzonuclease for 30 minutes, prior to boiling. Extracted proteins were separated by SDS-PAGE and transferred to PVDF or nitrocellulose membranes (Amersham Biosciences). After protein transfer, membranes were blocked in TBS-5% low fat milk (Elk, Campina, Amersfoort, the Netherlands) and stained with primary antibodies according to the specific antibody (Supplemental Table 5), washed in TBS-0.02% Tween, followed by IRDye conjugated secondary antibody (Li-cor, Biotechnology). Proteins were visualized with Odyssey®CLx (Li-cor, Biotechnology).

Ex vivo culture of patient derived xenografts

PDXs were generated as described by intrafemoral injection of 0.25 × 10^6 to 1 × 10^6 viable primary BCP-ALL cells in NOD.Cg-Prkdc^{scid}Il2rg^{tm1Wjl}/SzJ (NSG) mice(1). The *ex vivo* co-culture has been described previously(2). hTERT immortalized MSCs (3) were seeded in a 96-wells format (14,000 cells/well) 24 hours prior to the addition of ALL xenografts (140,000 cells/well) or ALL xenografts were seeded as mono-culture in case Zebularine was used (140,000 – 200,00 cells/well). ALL cells were allowed to settle for 24 hours before drugs was added in increasing concentrations. After 3 days of drug incubation, cells were stained with LIVE/DEAD™ Fixable Dead Cell Stain Sampler Kit (Thermo-Fischer, L34960) as described above. Cytogenetics of all PDX can be found in supplemental table 6.

In vivo mouse trial

This in vivo experiment was approved by the Animal Experimental Committee of the Radboud University (RU-DEC-2019-0036). Female Mice were housed in groups of 3-5 mice and cages were randomly distributed. For each leukemia, 2 mice NSG mice were randomly assigned and transplanted with 1.0 x 10^6 viable cells via intravenous injection and leukemia load was monitored by flow cytometric detection of human cells by staining blood samples for human CD10, CD45 and CD19 and murine CD45. When a particular sample reached a load of 1% human cells, mice were randomly assigned to treatment or control group and treated with 17,5 mg/kg cytarabine for two weeks (5 days on, 2 off treatment). Mice were weighed daily during treatment and weekly afterwards. Leukemia development was monitored by flow cytometry and the delay in growth was determined by calculating the reduction in time to event, defined as 30% of human cells in the blood. To account for differences in growth speed between leukemias, we first normalized all the times to leukemia and calculated the treatment related delay relative to this normalized growth.

Quantification of incorporated cytarabine by mass spectrometry

The method to determine DNA incorporated AraC was based on a LC-MS/MS method for the analysis of genomic DNA incorporated β-decitabine and 5-methyl-2'-deoxycytidine developed by J. Roosendaal et al(4). Sem wildtype and IKZF1$^{-/-}$ cells were seeded in triplicates and treated with either 1uM AraC for 24 hours or 30nM AraC for 72 hours. Genomic DNA was isolated using the DNA Blood mini kit (Qiagen) following manufactures protocol. Isolated DNA was degraded into single monophosphate nucleotides by adding 4 units of Nuclease P1 (Sigma-Aldrich, St. Louis, MO) and 100 µL digest buffer (0.04 mM deferoxamine mesylate, 3.25 mM ammonium acetate pH 5.0, 0.5 mM zinc chloride) to 50 µL of extracted DNA solution (ranged from 3.7 to 11.4µg DNA/50 µL in the measured samples) and incubated at 65°C for

10 min. The nucleotides were converted into nucleosides by adding 20 µL of 100 mM Trizma®base, pH 8.5 and 4 units of alkaline phosphatase (Roche Life Science, Indianapolis, IN) and incubating at 37°C for 1 h. After incubating, the reaction was stopped by adding 20 µL of 300 mM ammonium acetate pH 5.0 and 6 µL 0.25 mM DFOM/50 mM EDTA to the sample. 10 µL of internal standard working solution (containing 100 ng/mL cytarabine-$^{13}C_3$ and 10,000 ng/mL 2'-deoxycytidine [$^{13}C,^{15}N_2$] in water) was added to each sample before evaporating to dryness (40°C using and a gentle stream of nitrogen). The dry extract was reconstituted in 50 µL 5mM ammonium formate in ACN-water (98:2, v/v) by vortex mixing for 1 min.

Sample analysis was performed by injecting 10 µL of the processed sample onto the LC-MS system which consisted of an UPLC Acquity I Class pump, autosampler and column oven (Waters, Milford, MA,USA) coupled to a QTRAP5500 tandem mass spectrometer (Sciex, Framingham, MA, USA). Cytarabine and 2'-deoxycytidine were chromatographic separated on a Nova-Pak silica column (150 x 3.9 mm ID, 4 µm particle size from Waters, Milford, MA,USA) using a gradient elution with 5 mM ammonium formate in water (mobile phase A) and 5mM ammonium formate in ACN-water (98:2, v/v) (mobile phase B). The flow rate was 1.4 mL/min and a spitter (1:4) was used to introduce 25% of the flow in the QTRAP5500. The QTRAP5500 was equipped with a turbo ionspray interface and operated in positive ionization mode. Cytarabine (244.1→112.1), 2'-deoxycytidine (228.0→112.0), cytarabine-$^{13}C_3$ (347.1→115.1) and 2'-deoxycytidine [$^{13}C,^{15}N_2$] (231.0→115.0) were measured by multiple reaction monitoring. Since cytarabine and cytidine (endogenous nucleoside) are diastereomers, cytidine (244.101→112.1) was monitored to confirm that they were separated chromatographically. A correction for the amount of isolated and digested DNA was performed by expressing the DNA content of cytarabine as a cytarabine/2'-deoxycytidine ratio. Data acquisition was performed using Analyst 1.6.3 software (Sciex).

RNA sequencing

mRNA was isolated on triplicate samples using an RNeasy minikit (74106; Qiagen, Venlo, The Netherlands) after treatment with 1uM AraC for 16 hours. Sample sequencing and data analysis, including differential gene expression analysis, were performed by NovoGene (Cambridge, United Kingdom). Differentially expressed genes (FDR <0.05) of the following comparisons were combined for overrepresentation analysis: *IKZF1*^{wt} treated/*IKZF1*^{wt} untreated, *IKZF1*$^{-/-}$ untreated/*IKZF1*$^{-/-}$ treated, *IKZF1*^{wt} untreated/*IKZF1*$^{-/-}$ untreated and *IKZF1*^{wt} treated/*IKZF1*$^{-/-}$ treated. Overrepresentation analysis was performed in Rstudio using the clusterProfiler package, the Kyoto Encyclopedia of Genes and Genomes (KEGG) database. FDR values were calculated using the Benjamini&Hochberg multiple testing method. Heatmaps were created from FPKM values transformed into Z-scores and the ComplexHeatmap package.

Patient RNA expression data extracted from GSE87070

Log transformed microarray gene expression data from newly diagnosed pediatric ALL patients was derived from NCBI's Gene Expression Omnibus (GEO) data set GSE87070(5, 6) using additional subtype annotations and *IKZF1* deletion status (as available in R2, Supplemental Table 1). *IKZF1* copy number was annotated as either wildtype or deleted with no distinction between type of deletion. We included those BCP-ALL subtypes that have ≥ 4 patients with an *IKZF1* deletion making a cohort of in total n=252 patients wildtype for *IKZF1* and n=100 patients with an *IKZF1* deletion. Subtypes included are the high hyperdiploids (≥ 51 chromosomes) (Wildtype n=130, $IKZF1^{del}$ n=17), *BCR-ABL1* (Wildtype n=24, $IKZF1^{del}$ n=15), and B-other, defines as BCP-ALL negative for *ETV6-RUNX1*, high hyperdiploidy, *BCR-ABL1*, *KMT2A*-rearranged, *TCF3-PBX1* and *BCR-ABL1*-like signature (Wildtype n=198, $IKZF1^{del}$ n=68). Expression levels of SLC29A1 (hENT1) and MECOM (Evi1) were visualized using ggplot. The cut off for high *MECOM* expression was defined by the 95th percentile of *MECOM* expression in the *IKZF1* wildtype population. A Chi-square test was used to determine dependency of *IKZF1* status on MECOM expression. Expression levels of stemness markers were visualized using the ComplexHeatmap package and patients ordered based on MECOM expression.

Crispr/Cas9 screen

The kinase sgRNA library is used as earlier described(7). For this Crispr/Cas9 screen, Sem $IKZF1^{-/-}$ cells, previously transduced with Cas9, were now transduced with the kinase library at an MOI<1 and cells were selected using blasticidin. Cas9 expression was induced for 2 weeks by adding 1 ug/mL of doxycycline to the cells. Subsequently, cells were split in 3 pools of which 1 was left untreated and the others were exposed to 30nM and 50nM for a duration of 22 days, all in triplicates. To maintain library complexity, transduced cells were always cultured with a minimum of 1000 cells per guide, totaling to a minimum of 5 million cells per condition. After selection, genomic DNA was isolated from these pools and by PCR using Illumina barcode primers the sgRNA region was amplified (Supplemental Table 4). Then, sgRNA abundance was determined by deep sequencing on the Illumina Nextseq500 by the Utrecht sequencing facility, The Netherlands (USEQ). We confirmed that the library complexity was sufficiently maintained in samples at the start of the screen, before and after doxycycline treatment. Then, enriched and depleted genes were identified using the MAGeCK Test alogorithm (Galaxy Version 0.5.8.1)(8) (Supplemental Table 2).

Statistical analyses

All statistical analyses were performed using PRISM6 (GraphPad Software, La Jolla, CA). For the Amine staining, AUC was calculated of the dose response curves and either a two-tailed student's t test or ANOVA with ad hoc Turkey's multiple comparison test was performed. For

qRT-PCR, either a two-tailed student's t test was performed or ANOVA with ad hoc Turkey's multiple comparison test. On *in vivo* PDX data a two-sided student's T test is performed. For MRD patient data significance was tested by two sided Mann Whitney. For patient expression data extracted from R2, a Shapiro-Wilk test was performed to determine normality, followed by two sided Mann Whitney.

References

1. Schmitz M, Breithaupt P, Scheidegger N, Cario G, Bonapace L, Meissner B, Mirkowska P, Tchinda J, Niggli FK, Stanulla M. Xenografts of highly resistant leukemia recapitulate the clonal composition of the leukemogenic compartment. Blood, The Journal of the American Society of Hematology. 2011;118(7):1854-1864.

2. Frismantas V, Dobay MP, Rinaldi A, Tchinda J, Dunn SH, Kunz J, Richter-Pechanska P, Marovca B, Pail O, Jenni S. Ex vivo drug response profiling detects recurrent sensitivity patterns in drug-resistant acute lymphoblastic leukemia. Blood, The Journal of the American Society of Hematology. 2017;129(11):e26-e37.

3. Mihara K, Imai C, Coustan-Smith E, Dome JS, Dominici M, Vanin E, Campana D. Development and functional characterization of human bone marrow mesenchymal cells immortalized by enforced expression of telomerase. British journal of haematology. 2003;120(5):846-849.

4. Roosendaal J, Rosing H, Lucas L, Oganesian A, Schellens JH, Beijnen JH. Development, validation, and clinical application of a high-performance liquid chromatography-tandem mass spectrometry assay for the quantification of total intracellular β-decitabine nucleotides and genomic DNA incorporated β-decitabine and 5-methyl-2'-deoxycytidine. Journal of Pharmaceutical and Biomedical Analysis. 2019;164:16-26.

5. Polak R, Bierings MB, van der Leije CS, Sanders MA, Roovers O, Marchante JR, Boer JM, Cornelissen JJ, Pieters R, Den Boer ML. Autophagy inhibition as a potential future targeted therapy for ETV6-RUNX1-driven B-cell precursor acute lymphoblastic leukemia. Haematologica. 2019;104(4):738.

6. Jerchel IS, Boer JM, Hoogkamer AQ, Beverloo HB, Pieters R, den Boer ML. High PDGFRA expression does not serve as effective therapeutic target in ERG-deleted B-cell precursor acute lymphoblastic leukemia. Blood. 2017;130:1274.

7. Wang T, Wei JJ, Sabatini DM, Lander ES. Genetic screens in human cells using the CRISPR-Cas9 system. Science. 2014;343(6166):80-84.

8. Li W, Xu H, Xiao T, Cong L, Love MI, Zhang F, Irizarry RA, Liu JS, Brown M, Liu XS. MAGeCK enables robust identification of essential genes from genome-scale CRISPR/Cas9 knockout screens. Genome Biology. 2014 2014/12/05;15(12):554. doi:10.1186/s13059-014-0554-4.

SUPPLEMENTAL TABLES

Supplemental Table 1 Microarray gene expression data from NCBI's Gene Expression Omnibus (GEO) data set GSE87070 using additional subtype annotations and *IKZF1* deletion status provided as Excel file.

Supplemental Table 2 CRISPR-Cas9 screen results from MaGeck Test analysis: Ranking gene lists of depleted and enriched genes. Provided as Excel file.

Supplemental Table 3 *IKZF1* targeting gRNA sequences

Application	Name	Sequence
sgRNA	gRNA_IKZF1_exon3.1_FW	TCATCTGGAGTATCGCTTAC
	gRNA_IKZF1_exon3.2_FW	GACCTCTCCACCACCTCGGG
	gRNA_IKZF1_exon3.3_FW	CTCCAAGAGTGACAGAGTCG
	gRNA_control_FW	GTAGCGAACGTGTCCGGCGT

Supplemental Table 4 RT-qPCR and PCR primer sequences

Target	Use	Name	Sequence
ENT1	RT-qPCR	Forward primer	ACCTCAACTCCTTGCATCAGA
	RT-qPCR	Reverse primer	ACCAGGATGGCAGTGATCAGAAAC
Evi1	RT-qPCR	Forward primer	AGTGCCCTGGAGATGAGTTG
	RT-qPCR	Reverse primer	TTTGAGGCTATCTGTGAAGTGC
Kinase CRISPR/Cas9 screen	PCR	FW primer	AATGATACGGCGACCACCGAGATC TACACCGACTCGGTGCCACTTTT
	PCR	RV Barcode primer 1	CAAGCAGAAGACGGCATACGAGATC **ATCACG**TTTCTTGGGTAGTTTGCAGTTTT
	PCR	RV Barcode primer 2	CAAGCAGAAGACGGCATACGAGATC **CGATGT**TTTCTTGGGTAGTTTGCAGTTTT
		RV Barcode primer 3	CAAGCAGAAGACGGCATACGAGATC **TTAGGC**TTTCTTGGGTAGTTTGCAGTTTT
		RV Barcode primer 4	CAAGCAGAAGACGGCATACGAGATC **TGACCA**TTTCTTGGGTAGTTTGCAGTTTT
		RV Barcode primer 5	CAAGCAGAAGACGGCATACGAGATC **ACAGTG**TTTCTTGGGTAGTTTGCAGTTTT
		RV Barcode primer 6	CAAGCAGAAGACGGCATACGAGATC **GCCAAT**TTTCTTGGGTAGTTTGCAGTTTT
		RV Barcode primer 7	CAAGCAGAAGACGGCATACGAGATC **CAGATC**TTTCTTGGGTAGTTTGCAGTTTT
		RV Barcode primer 8	CAAGCAGAAGACGGCATACGAGATC **ACTTGA**TTTCTTGGGTAGTTTGCAGTTTT
		RV Barcode primer 9	CAAGCAGAAGACGGCATACGAGATC **GATCAG**TTTCTTGGGTAGTTTGCAGTTTT
		RV Barcode primer 10	CAAGCAGAAGACGGCATACGAGATC **TAGCTT**TTTCTTGGGTAGTTTGCAGTTTT
		RV Barcode primer 11	CAAGCAGAAGACGGCATACGAGATC **GGCTAC**TTTCTTGGGTAGTTTGCAGTTTT
		RV Barcode primer 12	CAAGCAGAAGACGGCATACGAGATC **CTTGTA**TTTCTTGGGTAGTTTGCAGTTTT
		RV Barcode primer 13	CAAGCAGAAGACGGCATACGAGATC **AGTCAA**TTTCTTGGGTAGTTTGCAGTTTT
		RV Barcode primer 14	CAAGCAGAAGACGGCATACGAGATC **AGTTCC**TTTCTTGGGTAGTTTGCAGTTTT
		RV Barcode primer 15	CAAGCAGAAGACGGCATACGAGATC **ATGTCA**TTTCTTGGGTAGTTTGCAGTTTT
		RV Barcode primer 16	CAAGCAGAAGACGGCATACGAGATC **CCGTCC**TTTCTTGGGTAGTTTGCAGTTTT
		RV Barcode primer 18	CAAGCAGAAGACGGCATACGAGATC **GTCCGC**TTTCTTGGGTAGTTTGCAGTTTT
		RV Barcode primer 19	CAAGCAGAAGACGGCATACGAGATC **GTGAAA**TTTCTTGGGTAGTTTGCAGTTTT
	Illumina sequencing	Read1 primer	CGGTGCCACTTTTTCAAGTTGATAACGGACTAG CCTTATTTTAACTTGCTATTTCTAGCTCTAAAAC
	Illumina sequencing	Index primer	TTTCAAGTTACGGTAAGCATATGATAGTCCATTTTA AAACATAATTTTAAAACTGCAAACTACCCAAGAAA

Supplemental Table 5 List of antibodies

Blocking and staining conditions for antibodies used in western blotting

Antibody	Supplier	Cat. number	Solvent	Dilution
actin	Sigma Aldrich	A4700	1% milk in TBS	1:10000
ENT1	Protein tech	11337-1-AP	1% milk in TBS	1:1000
Evi1	Cell Signaling	2265	1% milk in TBS	1:1000
Ikaros	Santa Cruz	sc-398265	1% milk in TBS	1:1000
PARP	Cell Signaling	9542	1% milk in TBS	1:4000
tubulin	Genetex	GTX628802	1% milk in TBS	1:10000
vinculin	Sigma Aldrich	V9131	1% milk in TBS	1:4000

Supplemental Table 6 Characteristics of BCP-ALL PDXs

Patient number	Cytogenetics	IKZF1 status	Sample type
#0202	TCF3-PBX1_ t(1::19)	Wildtype	Diagnosis
#2451	B-other	Wildtype	Diagnosis
#4818	Not available	Wildtype	Diagnosis
#0770	TP53 deletion	Wildtype	Diagnosis
#8153	TCF3-PBX1_ t(1::19)	Wildtype	Diagnosis
#6523	TCF3-PBX1_ t(1::19)	Wildtype	Diagnosis
#3862	TP53 deletion (25%), PAX5/CDKN2A	Wildtype	Diagnosis
#7148	TCF3-HLF_t(17::19)	Wildtype	Diagnosis
#2796	TCF3-HLF, t(17::19)	Wildtype	Diagnosis
#8076	TYK2	Wildtype	Diagnosis
#1502	ETV6-RUNX1	Wildtype	Diagnosis
#2103	TCF3-PBX1, t(1::19), PAX5 deletion 1-10	Wildtype	Diagnosis
#7811	BTG1 + IKZF1 deletion	Deletion	Diagnosis
#6609	IKZF1 deletion	Deletion	Diagnosis
#6439	BTG1 + IKZF1 deletion	Deletion	Diagnosis
#2072	IKZF1 deletion	Deletion	Diagnosis
#2400	IKZF1 deletion, PAX5 translocation	Deletion	Diagnosis
#3134	low hypodiploid, TP53 WT, IKZF1 deletion	Deletion	Diagnosis
#7558	IKZF1 deletion	Deletion	Diagnosis
#4707	EBF1deletion1-16, PAX5 deletion2-8, ETV6 deletion 1-2, IL3 deletion, CSF2RA, IKZF1deletion 4-7	Deletion	Diagnosis
#2377	ABL1+, CDKN2A/B deletion, PAX5 deletion, IKZF1 deletion 1-8, TP53 deletion	Deletion	Diagnosis
#6273	IKZF1 deletion 4-7, CDKN2A deletion	Deletion	Diagnosis
#2179	CRLF2, ETV6, IKZF1 deletion 2-3	Deletion	Diagnosis

SUPPLEMENTAL FIGURES

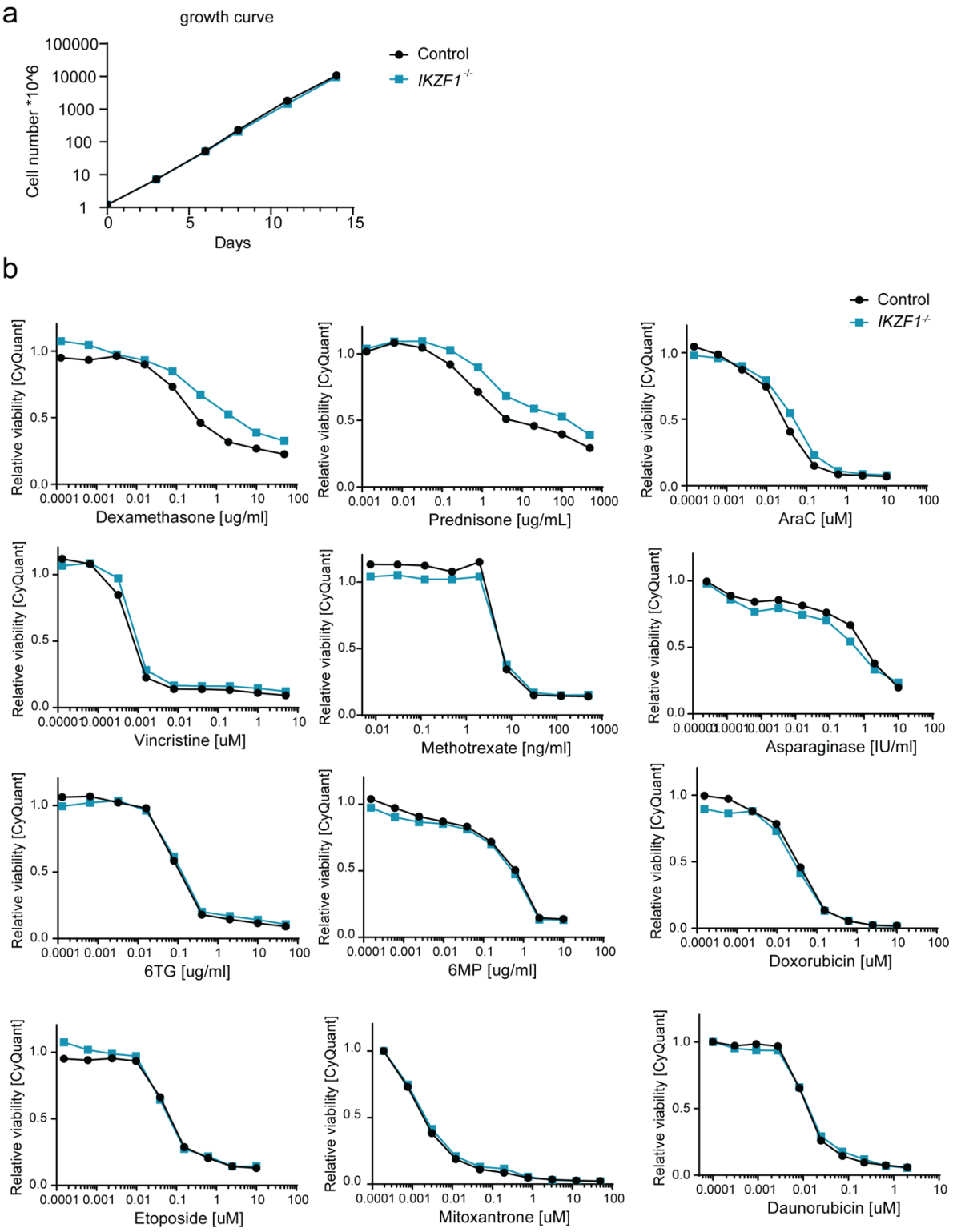
a
growth curve
Cell number *10^6
100000
10000
1000
100
10
1
0
5
10
15
Days
Control
IKZF1-/-
b
Control
IKZF1-/-
Relative viability [CyQuant]
Dexamethasone [ug/ml]
Prednisone [ug/mL]
AraC [uM]
Vincristine [uM]
Methotrexate [ng/ml]
Asparaginase [IU/ml]
6TG [ug/ml]
6MP [ug/ml]
Doxorubicin [uM]
Etoposide [uM]
Mitoxantrone [uM]
Daunorubicin [uM]

Supplemental Figure 1: CRISPR/Cas9-mediated targeting of *IKZF1* drives resistance to AraC

(a) Growth Curve of the Sem control versus *IKZF1*$^{-/-}$ cells (Mean ± SEM, n=3). **(b)** Relative viability as determined by a live cell staining using CyQuant in Sem control and Sem *IKZF1*$^{-/-}$ cells after a 3-day treatment with increasing concentrations (as indicated in figure) of different drugs used in the BCP-ALL treatment protocol.

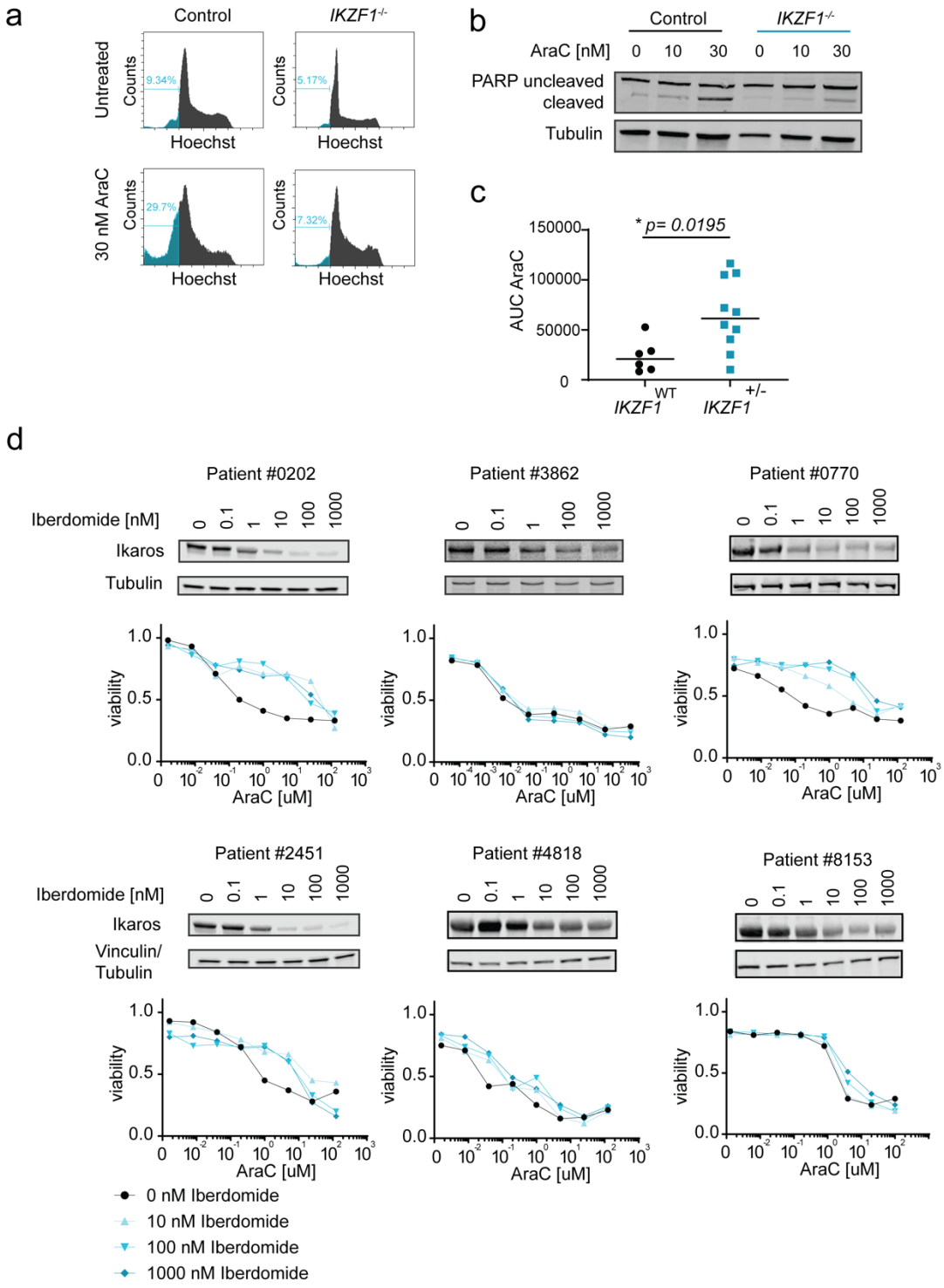

Supplemental Figure 2: Deletion of *IKZF1* drives resistance to AraC in Vitro

(a) AraC induced cell death as determined by quantification of cells in subG1 using flow cytometry of Hoechst-stained cells after a treatment of 30 nM AraC. Representative cell cycle distribution of three independent experiments. **(b)** Apoptosis induction upon AraC treatment measured by immunoblot analysis of PARP cleavage in Sem wt and Sem *IKZF1*$^{-/-}$ cells after a 3-day treatment with 0, 10 or 30 nM AraC. Representative blot of three independent

experiments. **(c)** Data from Figure 1f depicted as Area Under the Curve (AUC), (Mean ± SEM, **p*= *0.0195* unpaired T-test, two-tailed). **(d)** Collection of BCP-ALL PDX samples pharmacologically targeted by Iberdomide for degradation of the Ikaros protein. Immunoblot analysis of IKZF1 protein expression showing degradation of *IKZF1* protein in response to Iberdomide treatment after 24 hours. in different PDX samples. AraC induced cell death was determined by quantification of cells positive for amine-reactive dyes using flow cytometry after a 3-day treatment with increasing concentrations of AraC in the presence or absence of indicated doses of Iberdomide. Other tested PDX Samples (n=6) can be found in Supplemental figure 2d.

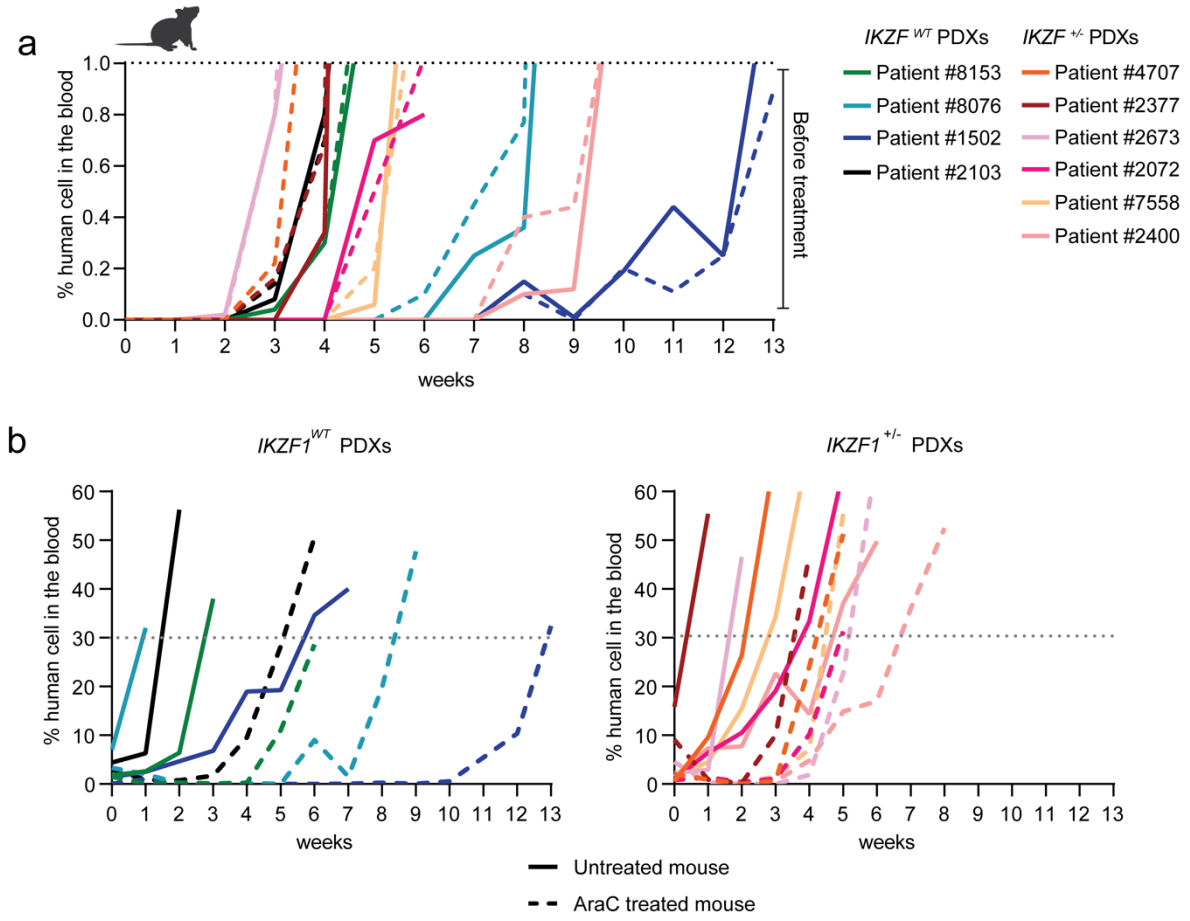

Supplemental Figure 3: In vivo Xenograft growth curves upon treatment with AraC **(a)** In vivo PDX growth curves, based on weekly measurement of % human cells in the blood from moment of Intravenous injection until start of treatment. Including here 4 PDX samples WT for *IKZF1* and 6 *IKZF1*$^{+/-}$ samples. **(b)** In vivo PDX growth curves, based on weekly measurement of % human cells in the blood, after treatment with either AraC or vehicle for 2 weeks until human endpoint was reached by either >50% of human cells in the blood, or based on condition of the mouse.

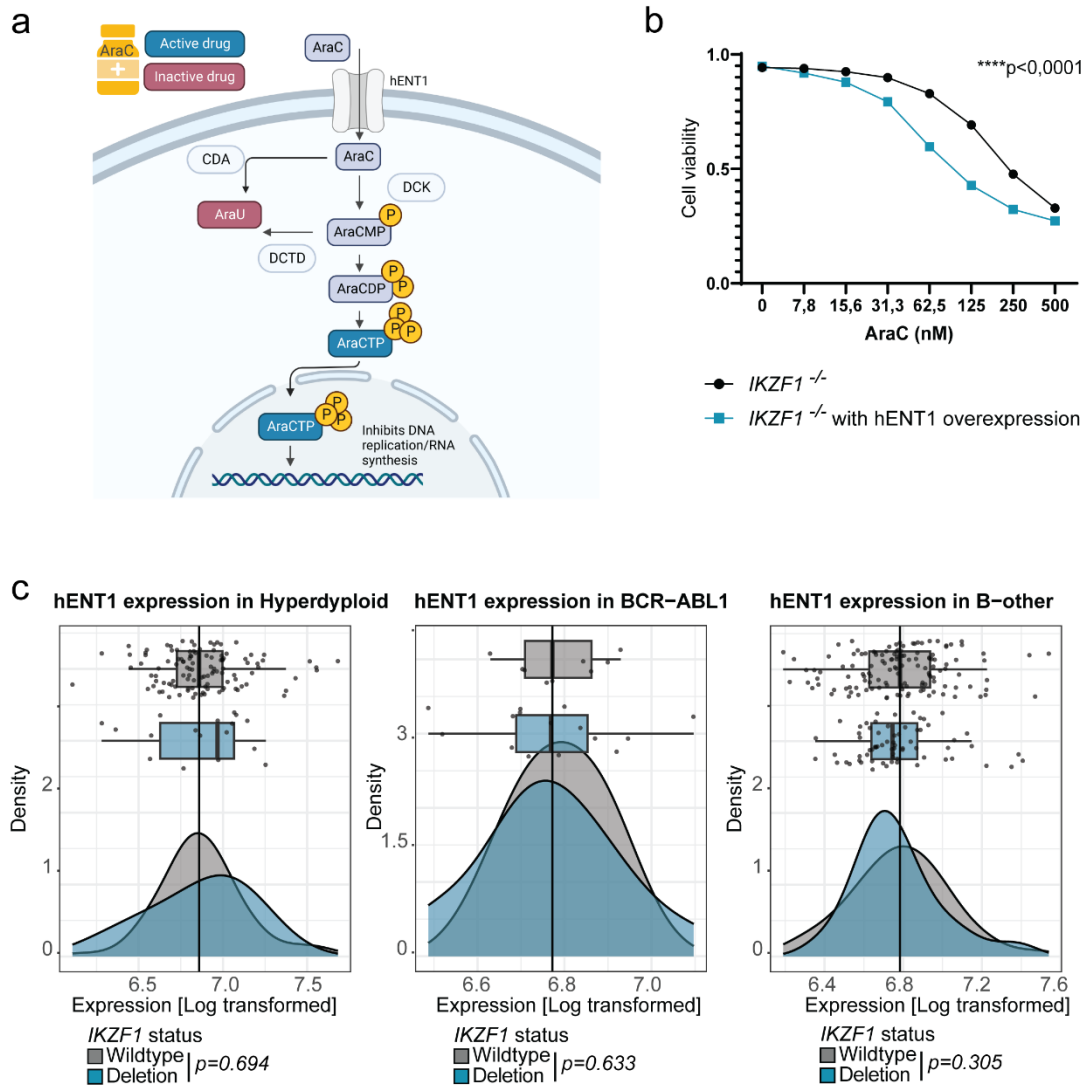

Supplemental Figure 4: the role of hENT1 in AraC metabolism and its expression in BCP-ALL subgroups

(a) Schematic representation of AraC metabolism by the cell, from cellular uptake to incorporated into DNA and RNA. Created with Biorender. **(b)** Dose response curve to 3 day AraC treatment in *IKZF1*$^{-/-}$ cells and IKZF-/- cells with an overexpression of EVI1. Each data point represents a mean (+/- SEM) of 2 independent experiments after 2 rounds of transduction. Student's T-test is performed on the AUC values (****p<0.0001) IC50 values shift from 141.6 nM to 59.4 nM AraC in cells with a hENT1 overexpression **(c)** hENT1 expression extracted from the GEO database, containing microarray gene expression data on patients harboring an *IKZF1* deletion versus patients wildtype for *IKZF1*. These plots illustrate the 3 subgroups hyperdiploid (n=130), BCR-ABL (n=24), B-other (n=198) that include >3 patients with an *IKZF1*^{del} deletion and are combined into one plot for Figure 3g.

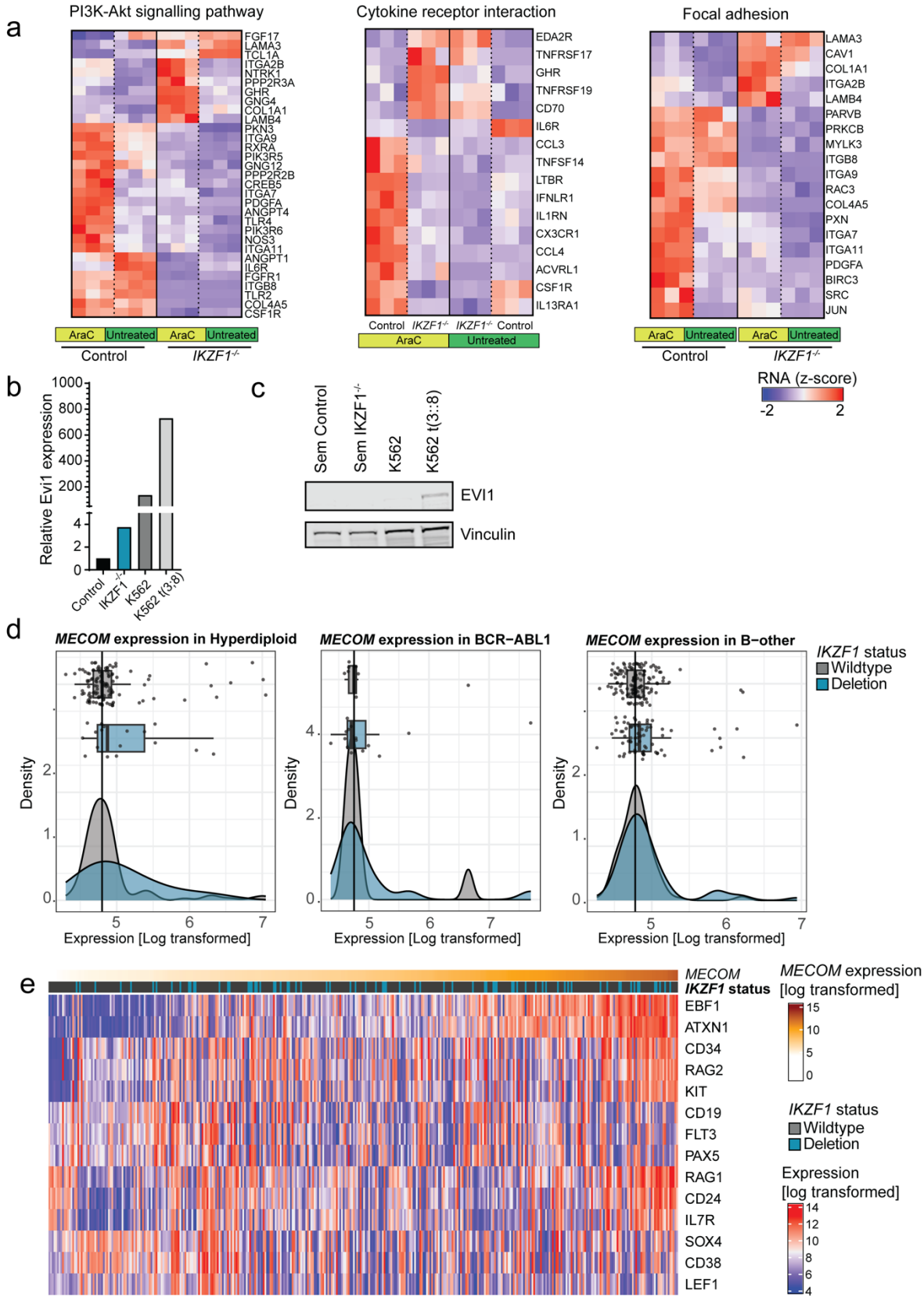
a
PI3K-Akt signalling pathway
FGF17
LAMA3
TCL1A
ITGA2B
NTRK1
PPP2R3A
GHR
GNG4
COL1A1
LAMB4
PKN3
ITGA9
RXRA
PIK3R5
GNG12
PPP2R2B
CREB5
ITGA7
PDGFA
ANGPT4
TLR4
PIK3R6
NOS3
ITGA11
ANGPT1
IL6R
FGFR1
ITGB8
TLR2
COL4A5
CSF1R
AraC
Untreated
AraC
Untreated
Control
IKZF1-/-
Cytokine receptor interaction
EDA2R
TNFRSF17
GHR
TNFRSF19
CD70
IL6R
CCL3
TNFSF14
LTBR
IFNLR1
IL1RN
CX3CR1
CCL4
ACVRL1
CSF1R
IL13RA1
Control
IKZF1-/-
IKZF1-/-
Control
AraC
Untreated
Focal adhesion
LAMA3
CAV1
COL1A1
ITGA2B
LAMB4
PARVB
PRKCB
MYLK3
ITGB8
ITGA9
RAC3
COL4A5
PXN
ITGA7
ITGA11
PDGFA
BIRC3
SRC
JUN
AraC
Untreated
AraC
Untreated
Control
IKZF1-/-
RNA (z-score)
-2
2
b
Relative Evi1 expression
1000
800
600
400
200
4
2
0
Control
IKZF1-/-
K562
K562 t(3;8)
c
Sem Control
Sem IKZF1-/-
K562
K562 t(3;8)
EVI1
Vinculin
d
MECOM expression in Hyperdiploid
MECOM expression in BCR−ABL1
MECOM expression in B−other
IKZF1 status
Wildtype
Deletion
Density
Expression [Log transformed]
e
MECOM
IKZF1 status
EBF1
ATXN1
CD34
RAG2
KIT
CD19
FLT3
PAX5
RAG1
CD24
IL7R
SOX4
CD38
LEF1
MECOM expression
[log transformed]
15
10
5
0
IKZF1 status
Wildtype
Deletion
Expression
[log transformed]
14
12
10
8
6
4

Supplemental Figure 5: Evi1 expression in different BCP-ALL subgroups and comparison to expression in AML

(a) Heatmaps created by unsupervised clustering of the PI3K-Akt, Cytokine receptor signaling and Focal adhesion pathway, only showing genes differentially expressed between control and *IKZF1*$^{-/-}$ cells upon AraC treatment. Heatmap is created using the FPKM values transformed into Z-scores. **(b)** Relative expression of Evi1 by RT-qPCR to determine relative expression of Evi1 between BCP-ALL cell line Sem and AML cell line K562. (Mean, n=2 technical replicate). **(c)** Immunoblot analysis of Evi1 protein expression in the BCP-ALL cell line Sem and the AML cell line K562. This is a representative blot of two independent experiments. **(d)** *MECOM* expression extracted from RNA sequencing on patients harboring an *IKZF1* deletion versus patients wildtype for *IKZF1*. These plots illustrate the 3 subgroups (hyper diploid (n=130), BCR-ABL (n=24), B-other (n=198) that include >3 patients with an *IKZF1*^{del} deletion and are combined into one plot for Figure 4G. **(e)** Log transformed RNA expression levels of stemness markers in patients either Wildtype for *IKZF1* or harboring a deletion. Patients of all BCP-ALL subtypes (hyper diploid, BCR-ABL, B-other) were combined and ordered based on *MECOM* expression (n=352).

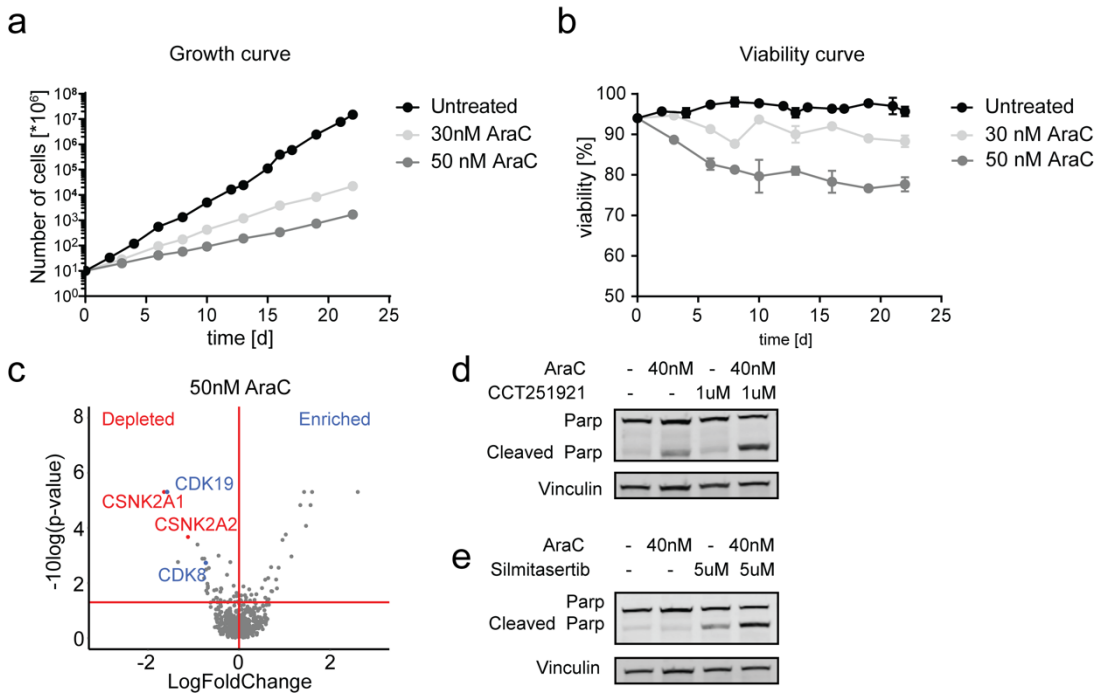

Supplemental Figure 6: Drug selection with AraC for kinase CRISPR/Cas9 screen

(a) Growth Curve of the Sem *IKZF1*$^{-/-}$ cells under selection of AraC for the CRISPR/Cas9 screen (Mean ± SEM, n=3). **(b)** Cell viability of the of the Sem *IKZF1*$^{-/-}$ cells under selection of AraC for the CRISPR/Cas9 screen (Mean ± SEM, n=3). **(c)** Vulcano-plot of gRNA targets that significantly modulate AraC response under selection of 50nM AraC. Genes are plotted based on p-value and log fold change as analyzed using the MaGeCK Test algorithm. **(d)** Apoptosis induction as measured by westernblot analysis of PARP cleavage in Sem *IKZF1*$^{-/-}$ cells after a 5-day treatment with AraC in combination with CCT251921. Representative blot of three independent experiments. **(e)** Apoptosis induction as measured by westernblot analysis of PARP cleavage in SEM *IKZF1*$^{-/-}$ cells after a 5-day treatment with AraC in combination with Silmitasertib. Representative blot of three independent experiments.